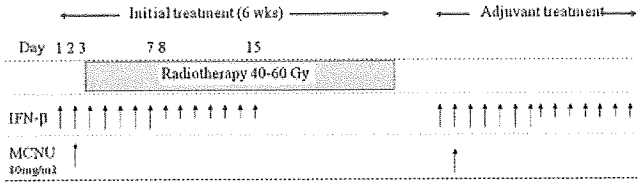

Fig. 1. Treatment regimen. Patients 1–10 received IFN-β at a daily dose of 1 million international units (MIU) on days 1–7, a reduced dose of 0.5 MIU on days 8–14, and MCNU at a dose of 80 mg/m^2 on day 2. Patients 11–15 received IFN-β at a daily dose of 2 MIU on days 1–7 and a reduced dose of 1 MIU on days 8–14. Radiotherapy was initiated to deliver radiation to the tumor bed from day 3 with a conventional fractionation of 1.5–2 Gy. Radiation was delivered once daily for 5 days per week to deliver a total dose of 40–60 Gy. The adjuvant administration of IFN-β and MCNU at the same dose was repeated every 6 weeks in cases with absence of tumor progression, with serious adverse events such as grade 4 hematological toxicity, and with refusal of therapy.

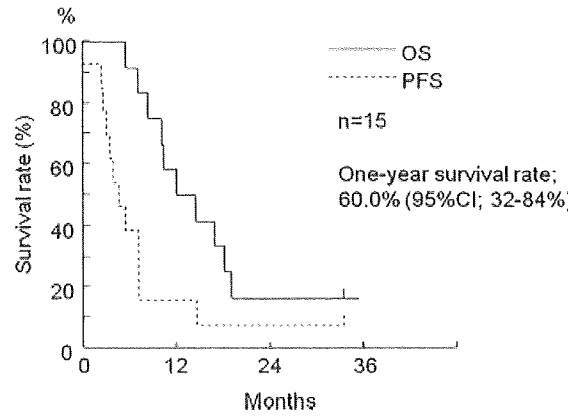

Fig. 2. The Kaplan–Meier curves of progression-free survival (PFS) and overall survival (OS). The median OS and the median PFS were 14.7 and 4.6 months, respectively.

from five brainstem tumor patients. These samples were obtained prior to surgery or chemoradiotherapy and were stored at −80°C. Serum DNA was prepared as described previously [9]. In brief, the serum sample was digested overnight with proteinase K and purified by following the phenol–chloroform extraction and ethanol precipitation protocol. After purification, 1 ml of the serum yielded an average of 50 ng of DNA. In order to analyze the MGMT promoter hypermethylation in the serum DNA, methylation-specific PCR (MSP) was performed as described in our previous publications [10,11]. Each PCR product (10 μl) was loaded onto a 3% agarose gel; the gel was stained with Ethidium bromide and directly visualized under ultraviolet (UV) illumination.

Statistical Methods

The studies were observational, non-randomized, and retrospective. The overall survival (OS) rates were calculated in years using the Kaplan–Meier method by employing SPSS for Windows, version 15.0.0 (SPSS, Inc., Chicago, IL). Survival was calculated from the initiation of combination chemotherapy to either the date of last follow-up or the date of death from any cause. The follow-up ended in September 2008.

RESULTS

Response Data

All patients were eligible for response evaluation after two rounds of therapy. Of the 15 patients, 5 patients had PR, 5 had ST, and 5 had PD (Table I). The objective response rate (CR + PR) of all patients in our series was 33.3%. Figure 2 shows the Kaplan–Meier curves of progression-free survival (PFS) and overall survival (OS). The median OS and the median PFS were 14.7 and 4.6 months, respectively. The 1-year survival rate was 60.0% (95% CI; 32–84%). At the end of this study, patient #13 who had experienced PR was alive, and the remaining 14 patients had died due to tumor progression. Seven patients received second-line chemotherapy, five received carboplatin (CBDCA) and oral etoposide (VP-16) therapy, and two received temozolomide. The patients also received conventional radiotherapy ranging from 45 to 60 Gy. However, second-line chemotherapy and the radiation dose did not exert any effects on tumor progression.

Toxicity

IMR therapy was generally well tolerated. Two patients had grade 3 AST/ALT elevation and one had grade 1 AST/ALT elevation. Five patients had neutropenia (Grade 3, two; Grade 2, two; and Grade 1, one). All patients with myelosuppression recovered within 2 weeks. No patients underwent termination of this protocol because of hematological toxicity, nephrotoxicity, or neurotoxicity. One patient suffered from meningitis due to postoperative cerebrospinal fluid leakage.

MGMT Methylation in Patients' Serum (Fig. 3)

Table I shows the MGMT promoter methylation status in the serum of five patients. A biopsy was performed in four of five patients. Among these patients, two had astrocytoma grade 1, one had astrocytoma grade 2, and one had astrocytoma grade 3. Patients with unmethylated MGMT promoter in their serum showed a PD response to IMR therapy, while MGMT promoter hypermethylation was observed in two PR patients and one SD patient. However, OS and PFS did not appear to correlate with the MGMT promoter methylation in the serum.

DISCUSSION

Therapeutic approaches to pontine gliomas continue to be extremely controversial. Radiotherapy is the only treatment indicated for diffusely infiltrating pontine gliomas, and treatment with local field radiotherapy amounting to a total dose of 54–60 Gy remains the best option as the standard treatment. The role of chemotherapy in the treatment of children with brainstem glioma is not well defined. Supplemental Table presents the results of clinical trials involving various chemotherapeutic regimens administered concurrently with or subsequent to radiotherapy. Prior to 2000, nitrosourea-based chemotherapy was the most frequently used treatment for brainstem glioma. Since 2000, platinum-based regimens with or without high-dose chemotherapy and autologous stem-cell rescue have been employed; however, these regimens did

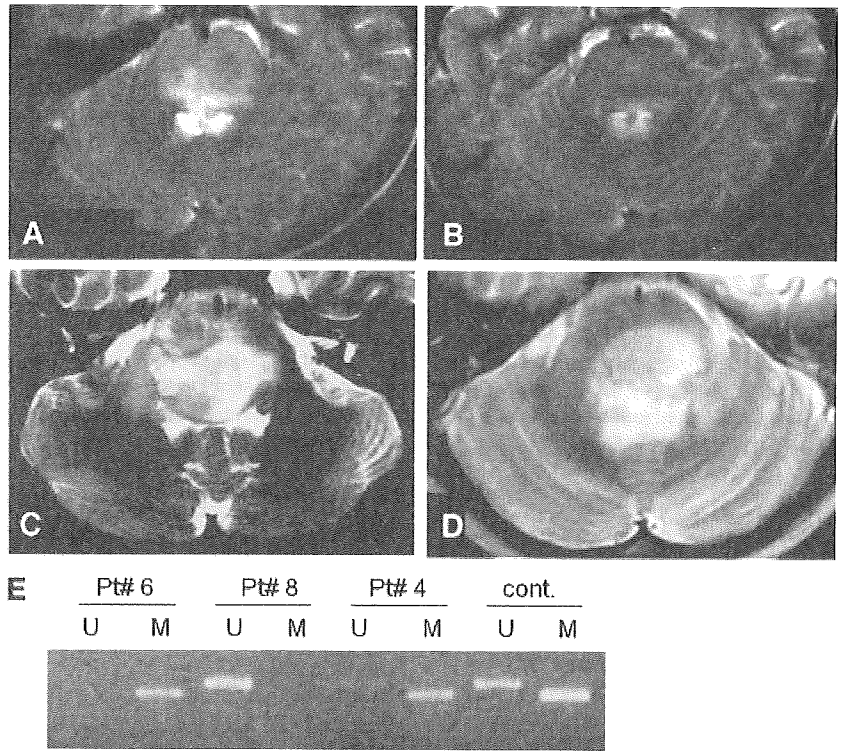

Fig. 3. Patient #6 (**A**,**B**). A 5-year-old boy presented with gait disturbance, right hemiparesis, and dysphasia. T2-weighted MRI revealed a high-intensity lesion in the pons (A). The patient received IFN-β at a daily dose of 1 MIU on days 1–7 and at a reduced dose of 0.5 MIU on days 8–14; she also received MCNU at a dose of 80 mg/m^2 on day 2. Radiotherapy was initiated to deliver radiation to the tumor bed from day 3 with a conventional fractionation of 1.5–2 Gy. Radiation was delivered once daily for 5 days per week to deliver a total dose of 60 Gy. The adjuvant administration of IFN-β and MCNU at the same dose was repeated every 6 weeks. Two months after the initial treatment, the patient's neurological symptoms improved, and the MRI revealed a remarkable reduction in the size of the T2-weighted high-intensity lesion (B). MGMT methylation in the serum DNA was positive (M) for this patient, as shown in panel **E**. Patient #8 (**C**,**D**). A 9-year-old boy presented with loss of consciousness, upward nystagmus, and ataxia. T2-weighted MRI revealed a high-intensity lesion involving the pons and medulla (C). The patient received IFN-β at a daily dose of 1 MIU on days 1–7 and a reduced dose of 0.5 MIU on days 8–14; he also received MCNU at a dose of 80 mg/m^2 on day 2. Radiotherapy was initiated to deliver radiation to the tumor bed from day 3 with a conventional fractionation of 1.5–2 Gy. Radiation was delivered once daily for 5 days per week to deliver a total dose of 59 Gy. Four months after the initial treatment, there was no improvement in his symptoms, and tumor progression (D) was detected on MRI. MGMT methylation in the serum DNA was negative (U) for this patient, as shown in panel E.

not appear to prolong survival to a greater extent than conventional radiotherapy. Recently, as temozolomide (TMZ) has become widely accepted for the treatment of adults with high-grade glioma, it has been used for the treatment of patients with newly diagnosed diffuse brainstem glioma to test the efficacy of TMZ administered concurrently with and subsequent to radiotherapy. However, response rates for these patients were lower than those observed for patients with adult supratentorial gliomas [12]. It was suggested that patients with brainstem tumors present with dysphasia at an early stage; therefore, the compliance of oral agents such as TMZ and VP-16 could be very limited. In this regard, the intravenous administration of nitrosoureas should be considered as an attractive treatment option for brainstem gliomas.

IFN-β exhibits pleiotropic biological effects and has been widely used either alone or in combination with other antitumor agents in the treatment of malignant gliomas and melanomas [13]. In the treatment of malignant gliomas, IFN-β can act as a drug sensitizer when administered in combination with nitrosourea. Combination therapy with IFN-β and nitrosourea has been widely employed for the treatment of gliomas in Japan [14]. In particular, our previous report suggested that a combination of chemotherapy plus interferon (IFN)-β and a different nitrosourea, 1-(4-amino-2-methyl-5-pyrimidinyl)-methyl-3-(2-chloroethyl)-3-nitrosourea hydrochloride (ACNU) along with radiation therapy (IAR therapy) may have a beneficial effect and may improve the radiological response rate in brainstem glioma patients [15]. With regard to the possible underlying molecular mechanism, we demonstrated that IFN-β markedly enhances chemosensitivity to alkylating agents in an in vitro study of human glioma cells [10]; this finding suggested that one of the major mechanisms by which IFN-β enhances chemosensitivity is the down-regulation of MGMT transcription via *p53* gene induction. Further, this effect was observed in an experimental animal model [11]. These studies suggested that chemotherapy with IFN-β and MCNU might improve the clinical outcome in brainstem gliomas. In this study, we demonstrated that the combination therapy of IFN-β and MCNU administered concurrently with and subsequent to radiotherapy was tolerable and the overall survival time achieved was over 12 months (median, 14.7 months); however, the limitation of this study is that it is a retrospective pilot study with a small sample size. Nonetheless, the efficacy of the

therapy regimen employed in this study may not be inferior to the efficacy reported in other recent pilot studies that employed molecular targeting agents such as tipifarnib [16].

Another interesting observation of this study is that three of five patients showed MGMT promoter hypermethylation in the serum DNA; further, these patients appeared to demonstrate radiological responses to the regimen employed in this study. The DNA-repair enzyme MGMT reduces the toxicity of alkylating agents because the transfer of alkyl groups to MGMT prevents the formation of lethal interstrand cross-links in DNA [17,18]. The subgroup of glioma patients with reduced MGMT activity showed enhanced sensitivity to alkylating agents [19]. Hypermethylation of the MGMT CpG island leads to MGMT transcriptional silencing, and the presence of MGMT methylation induces the lack of the MGMT protein [10]. To date, MGMT methylation in either the tumor or the serum has never been analyzed in cases of diffuse brainstem gliomas. Our observations may aid in the understanding of the genetic and molecular abnormalities associated with brainstem glioma and suggest that MGMT hypermethylation in the serum could be used as a non-invasive marker to predict the efficacy of alkylating agent-based chemotherapy for these tumors.

In summary, despite the above-mentioned limitations, the observations made from our series demonstrate that the combination therapy employed in this study is a promising treatment for brainstem glioma. The response to this treatment demonstrated by a small group of children with brainstem gliomas makes this combination therapy attractive for further studies.

REFERENCES

1. Stiller CA, Nectoux J. International incidence of childhood brain and spinal tumours. Int J Epidemiol 1994;23:458–464.
2. Fujisawa H, Reis RM, Nakamura M, et al. Loss of heterozygosity on chromosome 10 is more extensive in primary (de novo) than in secondary glioblastomas. Lab Invest 2000;80:65–72.
3. Gonzalez-Zulueta M, Bender CM, Yang AS, et al. Methylation of the 5′ CpG island of the p16/CDKN2 tumor suppressor gene in normal and transformed human tissues correlates with gene silencing. Cancer Res 1995;55:4531–4535.
4. Greger V, Passarge E, Hopping W, et al. Epigenetic changes may contribute to the formation and spontaneous regression of retinoblastoma. Hum Genet 1989;83:155–158.
5. Herman JG, Merlo A, Mao L, et al. Inactivation of the CDKN2/p16/MTS1 gene is frequently associated with aberrant DNA methylation in all common human cancers. Cancer Res 1995;55:4525–4530.
6. Merlo A, Herman JG, Mao L, et al. 5' CpG island methylation is associated with transcriptional silencing of the tumour suppressor p16/CDKN2/MTS1 in human cancers. Nat Med 1995;1:686–692.
7. Wakabayashi T, Natsume A, Hatano H, et al. p16 promoter methylation in the serum as a basis of the molecular diagnosis of gliomas. Neurosurgery (in press).
8. Choux MLG, Do L. Brainstem tumors. In: Choux M DRC, HockleyA, editors. Pediatric neurosurgery. New York: Churchill Livingstone; 2000. pp. 471–491.
9. Hibi K, Robinson CR, Booker S, et al. Molecular detection of genetic alterations in the serum of colorectal cancer patients. Cancer Res 1998;58:1405–1407.
10. Natsume A, Ishii D, Wakabayashi T, et al. IFN-beta down-regulates the expression of DNA repair gene MGMT and sensitizes resistant glioma cells to temozolomide. Cancer Res 2005;65:7573–7579.
11. Natsume A, Wakabayashi T, Ishii D, et al. A combination of IFN-beta and temozolomide in human glioma xenograft models: Implication of p53-mediated MGMT downregulation. Cancer Chemother Pharmacol 2008;61:653–659.
12. Broniscer A, Iacono L, Chintagumpala M, et al. Role of temozolomide after radiotherapy for newly diagnosed diffuse brainstem glioma in children: Results of a multiinstitutional study (SJHG-98). Cancer 2005;103:133–139.
13. Chawla-Sarkar M, Lindner DJ, Liu YF, et al. Apoptosis and interferons: Role of interferon-stimulated genes as mediators of apoptosis. Apoptosis 2003;8:237–249.
14. Wakabayashi T, Hatano N, Kajita Y, et al. Initial and maintenance combination treatment with interferon-beta, MCNU (Ranimustine), and radiotherapy for patients with previously untreated malignant glioma. J Neurooncol 2000;49:57–62.
15. Wakabayashi T, Yoshida J, Mizuno M, et al. Effectiveness of interferon-beta, ACNU, and radiation therapy in pediatric patients with brainstem glioma. Neurol Med Chir (Tokyo) 1992;32:942–946.
16. Haas-Kogan DA, Banerjee A, Kocak M, et al. Phase I trial of tipifarnib in children with newly diagnosed intrinsic diffuse brainstem glioma. Neuro-oncology 2008;10:341–347.
17. Ludlum DB. DNA alkylation by the haloethylnitrosoureas: Nature of modifications produced and their enzymatic repair or removal. Mutat Res 1990;233:117–126.
18. Pegg AE, Dolan ME, Moschel RC. Structure, function, and inhibition of O^6-alkylguanine-DNA alkyltransferase. Prog Nucleic Acid Res Mol Biol 1995;51:167–223.
19. Hegi ME, Diserens AC, Gorlia T, et al. MGMT gene silencing and benefit from temozolomide in glioblastoma. N Engl J Med 2005;352:997–1003.

Toshihiko Wakabayashi, M.D.
Center for Genetic and Regenerative Medicine, Nagoya University Hospital, Nagoya, Japan

Atsushi Natsume, M.D.
Department of Neurosurgery, Nagoya University School of Medicine, Nagoya, Japan

Hisashi Hatano, M.D.
Division of Neurosurgery, Meijo Hospital, Nagoya, Japan

Masazumi Fujii, M.D.
Department of Neurosurgery, Nagoya University School of Medicine, Nagoya, Japan

Shinji Shimato, M.D.
Department of Neurosurgery, Nagoya University School of Medicine, Nagoya, Japan

Motokazu Ito, M.D.
Department of Neurosurgery, Nagoya University School of Medicine, Nagoya, Japan

Masasuke Ohno, M.D.
Department of Neurosurgery, Nagoya University School of Medicine, Nagoya, Japan

Satoshi Ito, M.D.
Department of Neurosurgery, Nagoya University School of Medicine, Nagoya, Japan

Masatoshi Ogura, B.S.
Department of Neurosurgery, Nagoya University School of Medicine, Nagoya, Japan

Jun Yoshida, M.D.
Center for Genetic and Regenerative Medicine, Nagoya University Hospital, and Department of Neurosurgery, Nagoya University School of Medicine, Nagoya, Japan

Reprint requests:
Atsushi Natsume, M.D., Department of Neurosurgery, Nagoya University School of Medicine, 65 Tsurumai, Showa-ku, Nagoya 466-8550, Japan.
Email: anatsume@med.nagoya-u.ac.jp

Received, April 3, 2007.
Accepted, May 9, 2008.

Copyright © 2009 by the Congress of Neurological Surgeons

p16 PROMOTER METHYLATION IN THE SERUM AS A BASIS FOR THE MOLECULAR DIAGNOSIS OF GLIOMAS

OBJECTIVE: Deoxyribonucleic acid (DNA) methylation of tumor origin can be detected in the serum/plasma of cancer patients. The aim of this study was to detect aberrant *p16* promoter methylation as a potential diagnostic marker in the serum of patients with diffuse glioma to differentiate between gliomas and, particularly, to differentiate those in the brainstem from others; this was done by using the modified methylation-specific polymerase chain reaction technique.

METHODS: The methylation-specific polymerase chain reaction was used to detect *p16* methylation in the DNA extracted from 20 astrocytic tumors and 20 oligodendroglial tumors and the corresponding serum samples. Serum samples from 10 healthy individuals were used as controls. The association of *p16* hypermethylation in the serum DNA of glioma patients with clinicopathological characteristics was analyzed. In addition, the serum DNA in 7 patients with a brainstem tumor (4 gliomas, 1 schwannoma, 1 cavernous angioma, and 1 ependymoma) was analyzed.

RESULTS: We found *p16* methylation in 12 (60%) of the 20 tissues with astrocytoma, but in only 1 of the tissues with oligodendroglioma. Similar methylations were detected in the serum of 9 (75%) of the 12 patients with aberrant methylation in the tumor tissues. No methylated *p16* sequences were detected in the peripheral serum of the patients having tumors without these methylation changes or in the 10 healthy controls. Additionally, *p16* promoter methylation in the serum was observed in all brainstem astrocytoma cases, but not in other cases.

CONCLUSION: This assay has potential for use as a serum-based molecular diagnosis technique for diffuse glioma.

KEY WORDS: Glioma, Methylation, *p16*, Serum

Neurosurgery 64:455–462, 2009 DOI: 10.1227/01.NEU.0000340683.19920.E3 www.neurosurgery-online.com

Free deoxyribonucleic acid (DNA) can be detected in body fluids such as urine and serum. Two decades ago, it was first reported that DNA was present in the serum of patients with gastrointestinal cancer, and the amount of circulating DNA was correlated with the stage and status of metastasis (13, 24). In 1989, a technique that was based on the decreased strand stability of cancer cell DNA revealed that circulating serum DNA originated from cancer cells (30). Thereafter, a number of studies demonstrated that mutated or aberrant DNA (e.g., mutated *k-ras* and loss of heterozygosity [LOH]) of tumor origin was detected in the serum of patients with varieties of neoplasms, including central nervous system tumors (2, 27, 28).

It has been proven that the hypermethylation of a normally unmethylated CpG island in the promoter region of certain tumor suppressor genes such as *p16*, *RB*, and *DAPK* contributes to tumorigenesis (4–6, 8, 14). These experiments were carried out using the methylation-specific polymerase chain reaction (PCR), which is a sensitive and specific technique for methylation analysis. With this technique, DNA is amplified using primer pair sets to distinguish between methylated and unmethylated DNA by taking

ABBREVIATIONS: BST, brainstem tumor; **DNA**, deoxyribonucleic acid; **LOH**, loss of heterozygosity; **MGMT**, O6-methylguanine-DNA methyltransferase; **MSP**, methylation-specific polymerase chain reaction; **PCR**, polymerase chain reaction; **R^2**, coefficient of determination

advantage of sequence differences resulting from sodium bisulfite treatment, in which unmethylated cytosine is converted to uracil and methylated cytosine remains unchanged.

One interesting conclusion from most of these studies is that it is possible to detect alterations in the serum in the vast majority of cancer patients. This finding has opened up a number of possibilities for using these alterations in serum as a tool for detecting potential molecular markers, thus obviating the use of invasive tools for obtaining tumor tissues. To date, most of the studies published in the literature have analyzed the pattern of methylation only in serum or tissue, but in general, few reports have determined the correlation between the gene promoter methylation status of serum and tumor DNA obtained at the time of surgery (19).

The *CDKN2A* (*p16INK4a*) gene has been mapped to the short arm of chromosome 9 (9p21) and found to be aberrant in many different types of human cancers (21, 22), including anaplastic astrocytomas and glioblastomas (10, 23). *CDKN4A* encodes the p16INK4A protein, which functions as the regulator of the G_1-S phase transition by inhibiting the activity of the cyclin-dependent kinases Cdk4 and Cdk6 (22). In human neoplasms, the loss of *p16INK4A* expression may be caused by the homozygous deletion or hypermethylation of CpG islands in the promoter region. Among gliomas, the true frequency of *p16* hypermethylation remains controversial. Whereas Watanabe et al. (31) reported *p16* hypermethylation in only 1 of 49 oligodendrogliomas, Wolter et al. (32) demonstrated a higher frequency (32%) of hypermethylation in oligodendroglial tumors.

The goal of our study was to attempt to answer 3 interesting questions. First, does the methylation status of *p16* differ between astrocytic and oligodendroglial tumors? Second, is there a good correlation between such alterations in tumor and serum DNA? Third, can *p16* hypermethylation in the serum be useful to differentiate brainstem glioma from other types of histologies? Current diagnosis of brainstem tumors (BSTs) is performed largely by graphical examinations such as magnetic resonance imaging and positron emission tomography. Although biopsy provides a definitive histological diagnosis, owing to its invasive nature, the procedure cannot be applied in all cases. This limitation prompted us to develop noninvasive biomarkers for diagnosis of BSTs. In this study, we examined *p16* promoter hypermethylation in diffuse glioma samples and the corresponding serum samples by using the modified methylation-specific PCR (MSP) and compared their clinicopathological features. We found that this technique may be helpful for the serum-based differential diagnosis of gliomas.

PATIENTS AND METHODS

Patients

We retrospectively reviewed the newly diagnosed cases of 40 patients with nonbrainstem diffuse gliomas and 7 patients with BSTs who underwent surgery at the Nagoya University School of Medicine from 2000 to 2007. All patients had consented to the use of their tissue for research. Each patient's age at initial surgery, sex, smoking status, tumor location, histology, tumor size, and extent of surgical resection (biopsy, partial, or total resection) were recorded (Table 1). Particular attention was paid to the measurement of tumor volume and histology. The radiological features were carefully examined by magnetic resonance imaging before the initial operation. The volume measurement for each tumor was based on signal abnormalities detected on the set of T2-weighted sequences. The total volume of each tumor was calculated as the sum of the volumes of all regions traced on the set of magnetic resonance imaging scans. All tumors were histologically verified by at least 2 neuropathologists; among the patients with non-BSTs, 20 had astrocytic tumors (World Health Organization Grade II, 4; Grade III, 10; and Grade IV, 6), and 20 had oligodendroglial tumors (13 oligodendrogliomas [Grade II, 7; and Grade III, 6] and 7 oligoastrocytomas [Grade II, 3; and Grade III, 4]). In particular, because it is well known that that a majority of oligodendroglial tumors exhibit 1p/19q codeletion, astrocytic tumors with 1p and/or 19q losses were found, and oligodendroglial tumors without 1p and/or 19q losses were carefully reviewed by more than 2 neuropathologists.

Among patients with BSTs, 1 had a pilocytic astrocytoma (World Health Organization Grade I), 2 had a Grade II astrocytoma, 1 had a glioblastoma multiforme, 1 had a schwannoma, 1 had a cavernous angioma, and 1 had an ependymoma. The latter 3 tumors (schwannoma, cavernous angioma, and ependymoma) were located in the intrinsic pons, and on the basis of this finding, the predicted preoperative diagnosis was diffuse pontine astrocytoma.

Sample Collection and DNA Preparation

The molecular genetic analysis performed was approved by the institutional ethics committee of Nagoya University, and all of the patients who registered for this study provided written informed consent. We analyzed the serum samples from all patients and tumor samples from patients with non-BSTs. However, from BST patients, only 1 piece of tumor was obtained; it was sent for pathological examination, and therefore, no sample remained for the subsequent genetic analysis. All tissues were frozen immediately and stored at −80°C until analysis. The serum samples were obtained before surgery and stored at −80°C. In addition, 10 healthy volunteers comprising (6 men and 4 women; age range, 25–55 years; mean age, 43 years) provided serum samples for the normal control of this study. Tumor DNA was extracted using the QIAmp DNA mini kit (Qiagen, Hilden, Germany) in accordance with the manufacturer's instructions. Serum DNA was prepared as described previously (9). In brief, the serum sample was digested overnight with proteinase K and purified by phenol-chloroform extraction and ethanol precipitation. After purification, 1 mL of the serum yielded an average of 50 ng of DNA.

LOH Assay

We performed routine analysis of glioma for LOH using the ABI Prism 310 Genetic Analyzer (Applied Biosystems, Foster City, CA). The following microsatellite markers are located at the most frequently deleted sites in gliomas and were used for this assay: D1S244, D1S199, and D1S2734 for 1p (1p36) and D19S219, D19S412, and D19S112 for 19q (19q13) (20, 26, 29). The primer sequences for these markers are available in the Genome Database. The DNA extracted from each patient's leukocytes was used as the normal control and compared with the tumor DNA. In such a setting, if at least 1 of the 3 markers is informative, it can be used to distinguish LOH cases from non-LOH cases. The LOH result was considered positive if the allelic signal intensity in the tumor sample was reduced by more than 50% compared with that in the control.

Bisulfite Modification

The DNA obtained from the tumors and serum was subjected to bisulfite treatment as described previously (9). In brief, 1 μg of DNA

TABLE 1. Clinical and genetic features in glioma patients[a]

Patient no.	Age (y)/ sex	Smoking	Histology	Tumor location	Size (cm^3)	Surgery	1p loss	19q loss	p16 met (T)	p16 met (S)	MGMT met (T)	MGMT met (S)
1	16/F	NS	ASII	3rd ventricle	8	Partial	−	+	U	U	M	U
2	49/M	PS	ASII	Lt parietal	27	Total	−	−	U	U	U	U
3	35/M	CS	ASII	Rt temporal	35	Total	−	−	M	M	M	M
4	35/M	NS	ASII	Rt frontal	35	Total	−	−	M	U	U	U
5	40/M	CS	AA	CbII	18	Total	+	+	U	U	U	U
6	52/M	PS	AA	Bil frontal	20	Partial	−	+	M	M	M	M
7	37/F	NS	AA	Rt temporoparietal	30	Total	+	+	M	M	U	U
8	78/M	PS	AA	Bil frontal	75	Total	−	+	U	U	M	M
9	42/M	CS	AA	Lt temporal	24	Total	−	+	U	U	U	U
10	63/M	CS	AA	Lt frontal	25	Total	−	−	M	M	U	U
11	70/F	NS	AA	Rt temporal	78	Total	−	−	M	M	U	U
12	28/M	NS	AA	CbII	16	Partial	+	−	M	M	M	U
13	64/M	CS	AA	Lt frontal	42	Total	+	+	U	U	U	U
14	49/M	NS	AA	Rt frontal	20	Total	−	−	U	U	U	U
15	18/F	NS	GBM	Rt temporal	25	Total	−	−	M	M	U	U
16	59/M	PS	GBM	Lt frontal	25	Total	−	+	U	U	U	U
17	55/F	NS	GBM	Rt thalamus, brainstem	55	Total	−	+	M	U	U	U
18	17/M	NS	GBM	Lt thalamus, midbrain, lateral ventricle	28	Total	+	−	M	M	U	U
19	11/F	NS	GBM	Lt occipital	15	Total	−	−	M	U	M	M
20	66/M	CS	GBM	Lt temporal	8	Total	+	−	M	M	U	U
21	55/M	CS	OG	Lt frontal	120	Total	+	+	U	U	U	U
22	41/F	NS	OG	Lt frontal	2	Total	−	+	U	U	M	U
23	53/M	PS	OG	Rt frontal	36	Total	+	+	U	U	M	M
24	45/F	PS	OG	Lt frontal	3	Total	+	+	U	U	M	M
25	30/M	PS	OG	Lt frontal	12	Total	−	−	U	U	U	U
26	63/F	NS	OG	Rt frontal	25	Total	+	−	U	U	U	U
27	35/M	NS	OG	Lt frontal	10	Total	−	+	U	U	M	M
28	45/M	PS	OA	Lt frontal	70	Total	+	+	U	U	U	U
29	33/M	CS	OA	Lt frontal	60	Total	−	+	U	U	M	M
30	31/M	NS	OA	Rt parietal	6	Total	+	+	U	U	U	U
31	31/F	PS	AOG	Rt frontal	8	Total	+	+	U	U	M	U
32	70/F	NS	AOG	Bil frontal	6.5	Total	+	+	U	U	M	M
33	55/F	NS	AOG	Rt frontal	24	Total	+	+	U	U	U	U
34	46/M	PS	AOG	Rt frontal	8	Total	+	+	U	U	M	M
35	39/M	CS	AOG	Rt frontal	120	Total	+	−	U	U	U	U
36	64/M	CS	AOG	Rt parietal	30	Total	+	+	U	U	M	M
37	32/M	CS	AOA	Lt parietal	20	Total	+	+	U	U	M	M
38	45/F	CS	AOA	Rt frontal	1	Total	+	+	M	M	M	M
39	65/M	PS	AOA	Rt frontal	40	Total	−	−	U	U	U	U
40	35/M	CS	AOA	Bil frontal	90	Total	+	+	U	U	M	M

[a] met, methylation; T, tumor; S, serum; MGMT, O6-methylguanine-DNA methyltransferase; NS, never smoker; ASII, astrocytoma (World Health Organization Grade II); −, absent; +, present; U, unmethylated; M, methylated; PS, previous smoker; Lt, left; CS, current smoker; Rt, right; AA, anaplastic astrocytoma; CbII, cerebellum; Bil, bilateral; GBM, glioblastoma multiforme; OG, oligodendroglioma; OA, oligoastrocytoma; AOG, anaplastic oligodendroglioma; AOA, anaplastic oligoastrocytoma.

was denatured by NaOH and modified by sodium bisulfite. DNA samples were then purified using the Wizard purification resin (Promega, Madison, WI), treated once again with NaOH, precipitated with ethanol, and resuspended in water.

MSP for *p16* and O^6-Methylguanine-DNA Methyltransferase

The modified DNA was used as a template for MSP. The primer sequences of *p16* used in both MSPs were 5′-TTATTAGAGGG TGGGGTGGAT-TGT-3′ (sense) and 5′-CAACCCCAAACCACAA CATAA-3′ (antisense) for the unmethylated reaction and 5′-TTATTA-GAGGGTGGGGCGGATCGC-3′ (sense) and 5′-GACCCCGAACCGC-GACCGTAA-3′ (antisense) for the methylated reaction. The PCR condition was as follows: the PCR mixture contained 1× PCR buffer (1.5 mmol/L $MgCl_2$; Applied Biosystems), deoxynucleotide triphosphates (each at a concentration of 2 mmol/L), primers (500 nmol/L per reaction), *Taq* polymerase (0.5 unit per reaction; AmpliTaq Gold; Applied Biosystems), and bisulfite-modified DNA (50 ng) at a final volume of 20 μL. The reaction was hot-started at 95°C for 10 minutes. Amplification was carried out in a TaKaRa Thermal Cycler (Takara Shuzo Bio, Shiga, Japan) for 35 cycles (45 seconds at 95°C, 45 seconds at 60°C, and 60 seconds at 72°C). DNA from L132 (embryonic lung cell line) and H1299 (lung cancer cell line) was used as positive controls for unmethylated and methylated alleles, respectively. For the O^6-methylguanine-DNA methyltransferase (MGMT) promoter, MSP was performed as described in our previous publications (11, 17). Each PCR product (10 μL) was loaded onto a 3% agarose gel, stained with ethidium bromide, and directly visualized under ultraviolet illumination.

Statistical Analysis

The data were statistically analyzed by a χ^2 test to determine the difference in *p16* methylation status between astrocytoma and oligodendroglioma, and a Mann-Whitney *U* test was performed for the analysis of clinicoradiological features. To assess the coefficient of determination (R^2), standard logistic regression analysis was performed with SPSS software for Windows (Version 15.0.0; SPSS, Inc., Chicago, IL).

RESULTS

A More Frequent Detection of p16 Promoter Methylation in the Serum of Patients with Astrocytic Tumor Than in the Serum of Those with Oligodendroglial Tumor

To date, we have performed routine analysis of more than 200 samples of gliomas for LOH at 1p and 19q and *MGMT* promoter methylation. It is well known that that a majority of oligodendroglial tumors exhibit 1p/19q codeletion. Recent studies suggested that more than half of all oligodendroglial tumors exhibiting 1p LOH also show *MGMT* promoter methylation and a low MGMT level (1, 18). In this study as well, 65% of the oligodendroglial tumors that were histologically verified by more than 2 neuropathologists showed 1p/19q codeletion, whereas only 15% of the astrocytic tumors demonstrated these genetic alterations (Tables 1 and 2). There was a statistically significant difference between the 2 types of glioma in the distribution of the LOH status of 1p and 19q (Table 2). The R^2 value was 0.245, as explained on the basis of the LOH status (Table 2). The MGMT methylation in the tumor tissue was found in 60% of oligodendroglial tumors and 30% of astrocytic tumors, respectively ($P = 0.0587$, $R^2 = 0.088$) (Table 2). Although the serum testing found a greater significant difference between the 2 types of glioma ($P = 0.0481$, $R^2 = 0.096$), the difference was not so striking.

We next examined the methylation status of *p16* in tumor samples by using MSP. Notably, of the 20 astrocytic tumors, 12 (60%) exhibited abnormal promoter methylation of the *p16* gene, whereas 1 anaplastic oligoastrocytoma exhibited methylation (Tables 1 and 2). Subsequently, we examined whether aberrant methylation could be detected in the corresponding serum DNA of these patients with diffuse glioma. Of the 12 patients with *p16* promoter methylation in tumor DNA, 9 (75%) demonstrated abnormal methylation in their serum DNA,

TABLE 2. Association between tumor subtype and 1p/19q losses or *p16* methylation status[a]

Loss or methylation status	Astrocytic tumor (n = 20)		Oligodendroglial tumor (n = 20)		*P* value	R^2
	No.	%	No.	%		
LOH						
1p/19q codeletion	3	15%	13	65%		
1p deletion only	3	15%	2	10%		
19q deletion only	6	30%	3	15%		
No deletion of 1p/19q	8	40%	2	10%	0.0008	0.245
MGMT methylation						
(+) in tumor	6	30%	12	60%	0.0587	0.088
(+) in serum	4	20%	10	50%	0.0481	0.096
p16 methylation						
(+) in tumor	12	60%	1	5%	<0.0001	0.323
(+) in serum	9	45%	1	5%	0.0027	0.212

[a] LOH, loss of heterozygosity; MGMT, O^6-methylguanine-DNA methyltransferase; (+), present.

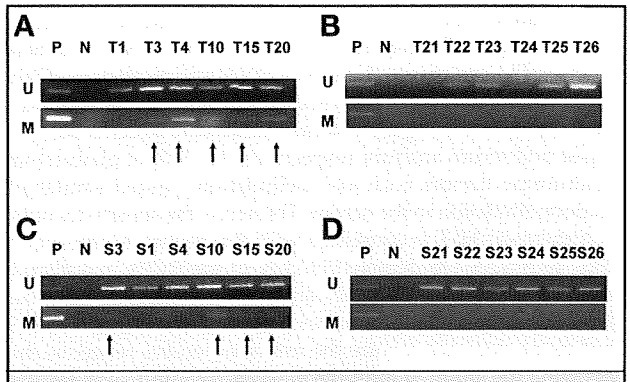

FIGURE 1. *Representative methylation-specific polymerase chain reaction (MSP) of* p16 *promoter in astrocytic tumors* (**A**)*, oligodendroglial tumors* (**B**)*, serum of patients with astrocytic tumors* (**C**)*, and serum of patients with oligodendroglial tumors* (**D**)*. Modified deoxyribonucleic acid from L132 and H1299 cell lines was used as a positive (P) control for unmethylated (U) and methylated (M) alleles, respectively. Water was used for a negative (N) control in each case. Arrow indicates a positive reaction in methylated alleles.*

whereas no methylation was found in the serum DNA of the 20 patients lacking tumor DNA methylation, or in the DNA of normal healthy volunteers. *p16* methylation was observed in the tumor and serum in the case of only 2 of 16 patients who had tumors with 1p/19q codeletions. Most importantly, the R^2 value increased from 0.245 to 0.396 when the serum *p16* methylation status was tested along with the 1p/19q LOH status. Representative results of the MSP analyses for *p16* promoter are shown in Figure 1.

The pathological stage and tumor size did not correlate with the representation of abnormal methylation in astrocytic tumors (Table 3). The abnormal methylation found in the low-grade astrocytoma was consistent with the finding that the aberrant methylation of *p16* is an early event in tumorigenesis (16). In addition, although cigarette smoking is known to be a background factor associated with the alterations in DNA methylation that occur during multistage carcinogenesis (12), in this study, the smoking status of the patients was not found to affect the incidence of *p16* methylation in both the tumor tissue and serum. Taken together, the presence of *p16* methylation in the serum may suggest an astrocytic tumor, although the absence of methylation provides no information about tumor histology.

Detection of *p16* Promoter Methylation in the Serum of Patients with Brainstem Glioma

Next, we examined the *p16* promoter methylation in the serum of 7 patients with a BST as a noninvasive biomarker. All tumors were histologically confirmed by biopsy or tumor removal surgery. Four were astrocytomas, and the other 3 tumors were a schwannoma, a cavernous angioma, and an ependymoma (Table 4). A representative case, BST 1, is presented in Figure 2, A and B. Interestingly, MSP showed no methylation of the *p16* promoter in the serum of nonastrocytoma patients, whereas other cases exhibited the methylation (Fig. 2C).

TABLE 3. Association between clinicopathology and *p16* methylation in astrocytic tumors[a]

	Tumor *p16* methylation		Serum *p16* methylation	
	+	−	+	−
Grade				
II	2	2	1	3
III	5	5	5	5
IV	5	1	3	3
P value	0.42		0.54	
Size				
Mean ± SD	28 ± 20	34 ± 18	34 ± 20	28 ± 19
Range	8–78	20–75	16–78	8–75
P value	0.28		0.38	
KPS				
Mean ± SD	93 ± 8	86 ± 12	93 ± 7	88 ± 12
Range	80–100	70–100	80–100	70–100
P value	0.19		0.38	
Smoking				
CS	4	9	4	9
PS	10	1	10	1
NS	8	8	5	11
P value	0.31		0.21	

[a] +, present; −, absent; SD, standard deviation; KPS, Karnofsky Performance Scale score; CS, currrent smoker; PS, previous smoker; NS, never smoked.

TABLE 4. Clinical features in patients with brainstem tumors[a]

Patient no.	Age (y)/sex	Histology	Size (cm^3)
BST 1	55/F	Schwannoma	4
BST 2	15/M	Cavernous angioma	2
BST 3	9/F	Astrocytoma I	3
BST 4	7/M	Astrocytoma II	2
BST 5	9/M	Astrocytoma II	2
BST 6	17/M	GBM	4
BST 7	9/F	Ependymoma	4

[a] BST, brainstem tumor; GBM, glioblastoma multiforme.

DISCUSSION

Changes in the methylation status play an important role in tumorigenesis. In particular, the hypermethylation of the normally unmethylated CpG islands in some tumor suppressor genes is associated with loss of expression (3). To study the

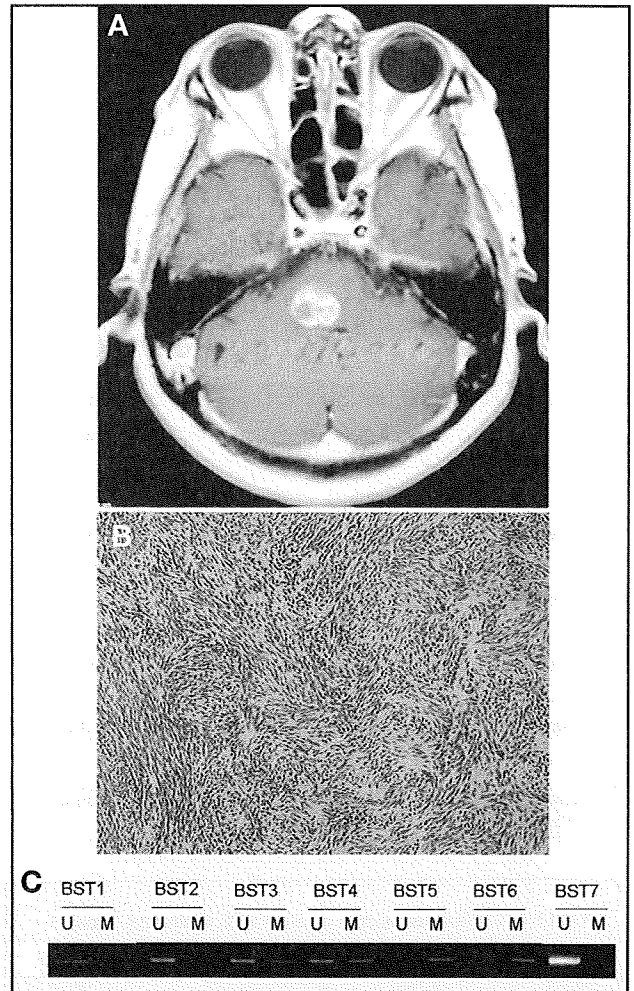

FIGURE 2. *Brainstem tumor (BST) cases. The BST 1 patient presented with a history of vertigo for a duration of approximately 1 month.* **A**, *magnetic resonance imaging (MRI) scan revealing an irregularly enhancing lesion with partial hemorrhage in the pons and the medulla. The possible preoperative diagnosis, based on the MRI scan, was a glioma or an angioma. The patient underwent a partial resection by a transcondylar approach.* **B**, *photomicrograph showing that the tumor was composed predominantly of Antoni A tissue with spindle-form cells.* **C**, *MSP showing no methylation (U lanes) of the* p16 *promoter in the serum of patients with nonastrocytoma tumors (BST 1, 2, and 7), whereas other glioma cases (BST 3–6) exhibited the methylation (M lanes).*

genes inactivated by the hypermethylation of promoters in cancers, the MSP technique was used because it is simple and highly sensitive, i.e., it is capable of detecting 1 methylated gene copy among 1000 unmethylated copies in dilution experiments (7). In our preliminary experiment, we used a limiting dilution of human placental DNA treated with SssI methyltransferase to serve as the positive control for methylated alleles, and the methylated *p16* promoter could be observed at up to a 10 000-fold dilution (data not shown). Hence, we could detect aberrant methylation in the plasma or serum DNA in 9 of 12 patients whose *p16* promoter in the tumor DNA was methylated (Table 1). Ramirez et al. (19) observed *p16* promoter methylation in 66.7% and 53.6% of glioblastoma multiforme patients based on tissue and serum analysis, respectively, i.e., 80% of glioblastoma multiforme tumors with *p16* methylation yielded similar *p16* hypermethylation in the serum. Therefore, the sensitivity of our serum-based MSP is consistent with this report. Moreover, the MSP technique has demonstrated great specificity in our study, and we did not find any abnormal methylation in the serum DNA if this methylation was not present in the tumor. The MSP technique does not require the use of expensive reagents, thus allowing the study of multiple markers by rapid analysis.

The *p16* methylation in serum DNA, in particular, may be a useful marker for the diagnosis of astrocytic tumors because we could detect *p16* methylation in the serum DNA of 9 (45%) of 20 patients with astrocytic tumors but in only 1 of the patients with oligodendroglial tumors. However, a limitation regarding the use of this potential marker is that the absence of serum *p16* methylation cannot be used as an indicator of a histological difference between astrocytomas and oligodendrogliomas.

Another interesting observation in the present study is that *p16* hypermethylation was detected in the serum of patients with brainstem astrocytomas, but not in the serum of those with tumors of other histologies. Because several studies have suggested that infratentorial gliomas may have different genetics from supratentorial ones (25), the detection of serum *p16* methylation in brainstem gliomas would be of interest in the context of this study. Additionally, we measured the *p16* promoter methylation in the serum of 44 patients with meningiomas (15). The result revealed that, regardless of the location and World Health Organization grade of the tumor, the serum of all of the meningioma patients was negative for *p16* methylation (data not shown).

This technique may be applied to differentiate brainstem gliomas from other types of histology. However, it is necessary to conduct a study with a larger population, in which the hypothesis that the detection of *p16* promoter methylation in the serum is a useful tool to support the diagnosis of brainstem gliomas will be tested in a more systematic manner. Alternatively, the analysis of abnormal promoter methylation status of several genes, in combination with the study of previously described gene alterations, may improve the specificity of the molecular diagnosis in which serum DNA is used. In addition, the serial studies of *p16* methylation in serum DNA may be useful in monitoring the response of adjuvant therapies, including chemoradiotherapy. The study of *p16* methylation of serum DNA may have great potential for monitoring relapse during follow-up. For example, neurosurgeons often encounter malignant gliomas that are difficult to categorize as a relapse or radiation-induced necrosis. Furthermore, serum-based molecular analysis may be used in the future for the selection of treatment. Considering *MGMT* methylation, which is correlated with the efficacy of alkylating agents, its measurement in the blood may be clinically relevant with regard to treatment options involving the use of MGMT-

targeting drugs in the near future. These issues will be addressed in our next study. Although the results of this study are still preliminary, the number of cases studied is small, and further prospective testing in a clinical setting is necessary, this technique has great potential because it allows the sensitive and accurate detection of circulating methylated *p16* promoter DNA.

Disclosure

The authors have no personal financial or institutional interest in any of the drugs, materials, or devices described in this article

REFERENCES

1. Branle F, Lefranc F, Camby I, Jeuken J, Geurts-Moespot A, Sprenger S, Sweep F, Kiss R, Salmon I: Evaluation of the efficiency of chemotherapy in in vivo orthotopic models of human glioma cells with and without 1p19q deletions and in C6 rat orthotopic allografts serving for the evaluation of surgery combined with chemotherapy. **Cancer** 95:641–655, 2002.
2. Chen X, Bonnefoi H, Diebold-Berger S, Lyautey J, Lederrey C, Faltin-Traub E, Stroun M, Anker P: Detecting tumor-related alterations in plasma or serum DNA of patients diagnosed with breast cancer. **Clin Cancer Res** 5:2297–2303, 1999.
3. Esteller M: Relevance of DNA methylation in the management of cancer. **Lancet Oncol** 4:351–358, 2003.
4. Fujisawa H, Reis RM, Nakamura M, Colella S, Yonekawa Y, Kleihues P, Ohgaki H: Loss of heterozygosity on chromosome 10 is more extensive in primary (de novo) than in secondary glioblastomas. **Lab Invest** 80:65–72, 2000.
5. Gonzalez-Zulueta M, Bender CM, Yang AS, Nguyen T, Beart RW, Van Tornout JM, Jones PA: Methylation of the 5′ CpG island of the p16/CDKN2 tumor suppressor gene in normal and transformed human tissues correlates with gene silencing. **Cancer Res** 55:4531–4535, 1995.
6. Greger V, Passarge E, Höpping W, Messmer E, Horsthemke B: Epigenetic changes may contribute to the formation and spontaneous regression of retinoblastoma. **Hum Genet** 83:155–158, 1989.
7. Herman JG, Graff JR, Myöhänen S, Nelkin BD, Baylin SB: Methylation-specific PCR: A novel PCR assay for methylation status of CpG islands. **Proc Natl Acad Sci U S A** 93:9821–9826, 1996.
8. Herman JG, Merlo A, Mao L, Lapidus RG, Issa JP, Davidson NE, Sidransky D, Baylin SB: Inactivation of the *CDKN2/p16/MTS1* gene is frequently associated with aberrant DNA methylation in all common human cancers. **Cancer Res** 55:4525–4530, 1995.
9. Hibi K, Robinson CR, Booker S, Wu L, Hamilton SR, Sidransky D, Jen J: Molecular detection of genetic alterations in the serum of colorectal cancer patients. **Cancer Res** 58:1405–1407, 1998.
10. Ichimura K, Bolin MB, Goike HM, Schmidt EE, Moshref A, Collins VP: Deregulation of the p14ARF/MDM2/p53 pathway is a prerequisite for human astrocytic gliomas with G1-S transition control gene abnormalities. **Cancer Res** 60:417–424, 2000.
11. Ishii D, Natsume A, Wakabayashi T, Hatano H, Asano Y, Takeuchi H, Shimato S, Ito M, Fujii M, Yoshida J: Efficacy of temozolomide is correlated with 1p loss and methylation of the deoxyribonucleic acid repair gene MGMT in malignant gliomas. **Neurol Med Chir (Tokyo)** 47:341–350, 2007.
12. Kanai Y, Hirohashi S: Alterations of DNA methylation associated with abnormalities of DNA methyltransferases in human cancers during transition from a precancerous to a malignant state. **Carcinogenesis** 28:2434–2442, 2007.
13. Leon SA, Shapiro B, Sklaroff DM, Yaros MJ: Free DNA in the serum of cancer patients and the effect of therapy. **Cancer Res** 37:646–650, 1977.
14. Merlo A, Herman JG, Mao L, Lee DJ, Gabrielson E, Burger PC, Baylin SB, Sidransky D: 5′ CpG island methylation is associated with transcriptional silencing of the tumour suppressor p16/CDKN2/MTS1 in human cancers. **Nat Med** 1:686–692, 1995.
15. Nakane Y, Natsume A, Wakabayashi T, Oi S, Ito M, Inao S, Saito K, Yoshida J: Malignant transformation-related genes in meningiomas: Allelic loss on 1p36 and methylation status of p73 and RASSF1A. **J Neurosurg** 107:398–404, 2007.
16. Nakayama H, Hibi K, Takase T, Yamazaki T, Kasai Y, Ito K, Akiyama S, Nakao A: Molecular detection of p16 promoter methylation in the serum of recurrent colorectal cancer patients. **Int J Cancer** 105:491–493, 2003.
17. Natsume A, Ishii D, Wakabayashi T, Tsuno T, Hatano H, Mizuno M, Yoshida J: IFN-β down-regulates the expression of DNA repair gene MGMT and sensitizes resistant glioma cells to temozolomide. **Cancer Res** 65:7573–7579, 2005.
18. Nutt CL, Noble M, Chambers AF, Cairncross JG: Differential expression of drug resistance genes and chemosensitivity in glial cell lineages correlate with differential response of oligodendrogliomas and astrocytomas to chemotherapy. **Cancer Res** 60:4812–4818, 2000.
19. Ramirez JL, Taron M, Balaña C, Sarries C, Mendez P, de Aguirre I, Nuñez L, Roig B, Queralt C, Botia M, Rosell R: Serum DNA as a tool for cancer patient management. **Rocz Akad Med Bialymst** 48:34–41, 2003.
20. Rosenberg JE, Lisle DK, Burwick JA, Ueki K, von Deimling A, Mohrenweiser HW, Louis DN: Refined deletion mapping of the chromosome 19q glioma tumor suppressor gene to the D19S412-STD interval. **Oncogene** 13:2483–2485, 1996.
21. Roussel MF: The INK4 family of cell cycle inhibitors in cancer. **Oncogene** 18:5311–5317, 1999.
22. Ruas M, Peters G: The p16INK4a/CDKN2A tumor suppressor and its relatives. **Biochim Biophys Acta** 1378:F115–F177, 1998.
23. Schmidt EE, Ichimura K, Reifenberger G, Collins VP: CDKN2 (p16/MTS1) gene deletion or CDK4 amplification occurs in the majority of glioblastomas. **Cancer Res** 54:6321–6324, 1994.
24. Shapiro B, Chakrabarty M, Cohn EM, Leon SA: Determination of circulating DNA levels in patients with benign or malignant gastrointestinal disease. **Cancer** 51:2116–2120, 1983.
25. Sharma MK, Mansur DB, Reifenberger G, Perry A, Leonard JR, Aldape KD, Albin MG, Emnett RJ, Loeser S, Watson MA, Nagarajan R, Gutmann DH: Distinct genetic signatures among pilocytic astrocytomas relate to their brain region origin. **Cancer Res** 67:890–900, 2007.
26. Smith JS, Perry A, Borell TJ, Lee HK, O'Fallon J, Hosek SM, Kimmel D, Yates A, Burger PC, Scheithauer BW, Jenkins RB: Alterations of chromosome arms 1p and 19q as predictors of survival in oligodendrogliomas, astrocytomas, and mixed oligoastrocytomas. **J Clin Oncol** 18:636–645, 2000.
27. Sorenson GD, Pribish DM, Valone FH, Memoli VA, Bzik DJ, Yao SL: Soluble normal and mutated DNA sequences from single-copy genes in human blood. **Cancer Epidemiol Biomarkers Prev** 3:67–71, 1994.
28. Sozzi G, Conte D, Mariani L, Lo Vullo S, Roz L, Lombardo C, Pierotti MA, Tavecchio L: Analysis of circulating tumor DNA in plasma at diagnosis and during follow-up of lung cancer patients. **Cancer Res** 61:4675–4678, 2001.
29. Steck PA, Pershouse MA, Jasser SA, Yung WK, Lin H, Ligon AH, Langford LA, Baumgard ML, Hattier T, Davis T, Frye C, Hu R, Swedlund B, Teng DH, Tavtigian SV: Identification of a candidate tumour suppressor gene, MMAC1, at chromosome 10q23.3 that is mutated in multiple advanced cancers. **Nat Genet** 15:356–362, 1997.
30. Stroun M, Anker P, Maurice P, Lyautey J, Lederrey C, Beljanski M: Neoplastic characteristics of the DNA found in the plasma of cancer patients. **Oncology** 46:318–322, 1989.
31. Watanabe T, Nakamura M, Yonekawa Y, Kleihues P, Ohgaki H: Promoter hypermethylation and homozygous deletion of the p14ARF and p16INK4a genes in oligodendrogliomas. **Acta Neuropathol** 101:185–189, 2001.
32. Wolter M, Reifenberger J, Blaschke B, Ichimura K, Schmidt EE, Collins VP, Reifenberger G: Oligodendroglial tumors frequently demonstrate hypermethylation of the CDKN2A (MTS1, p16INK4a), p14ARF, and CDKN2B (MTS2, p15INK4b) tumor suppressor genes. **J Neuropathol Exp Neurol** 60:1170–1180, 2001.

Acknowledgment

We thank Hisae Kanai for her technical assistance.

COMMENTS

In this study, Wakabayashi et al. measured *p16* methylation in the deoxyribonucleic acid (DNA) extracted from both tumors and serum in an attempt to correlate p16 hypermethylation with tumor pathology. They looked at 40 non-brainstem gliomas (20 astrocytomas and 20

oligodendrogliomas), as well as 6 brainstem lesions (4 gliomas, 1 schwannoma, and 1 cavernous angioma).

For the non-brainstem tumors (n = 40), the authors show that aberrant methylation of selected CpG sites in the *p16* gene correlates with astrocytic tumors (12 of 20) but is not significantly associated with oligodendroglial tumors (1 of 20) nor found in the serum of healthy control subjects (n = 10). There are a number of differences between astrocytomas and oligodendrogliomas, including prognosis and response to therapy. The authors demonstrate yet another potential difference in astrocytomas versus oligodendrogliomas, showing that hypermethylation of the *p16* gene in the tumor tissue and the serum may be diagnostic of astrocytomas. The results of this part of the study suggest that, with respect to histopathological classification, a statistically significant difference exists in the level of *p16* methylation between astrocytic tumors and oligodendroglial tumors (Table 2), which could be discernible in both the tumor tissue and/or the serum. In this part of the study, the analysis was well controlled, with serum from 10 healthy control subjects. Samples were defined as methylated on *p16* by the presence of a polymerase chain reaction product from a methylation-specific primer set. This section of the study was nicely done, and the technique described by the authors has the potential to play a role as an additional diagnostic tool for neurosurgeons and neuro-oncologists in differentiating between astrocytic and oligodendroglial gliomas.

For the patients with brainstem tumors (n = 6), the authors attempt to show that *p16* methylation detected in the serum of these patients was diagnostic of gliomas versus other types of brainstem lesions. The data presented in this part of the study are much less convincing. Of the patients with brainstem lesions analyzed for serum *p16* methylation, only 2 were negative. These happened to include 1 patient with schwannoma and 1 with a cavernous angioma. The authors conclude, on the basis of these 2 incidental cases, that "this technique may be applied to differentiate brainstem gliomas from other types of histology." This conclusion cannot be made from these anecdotal cases of a non-glioma brainstem lesion that happened to have undetectable serum *p16* methylation. The inability to detect some level of aberrant methylation in the serum is not necessarily a direct reflection of the *p16* methylation level in the tumor tissue, because there are a number of barriers that might prevent accurate detection of gene methylation in serum. More negative controls (i.e., other types of brainstem tumors) need to be tested in order for the authors to tout *p16* hypermethylation as a serum biomarker for brainstem gliomas.

Overall, this is a nice report, and the data raise some interesting questions for further study. The first part of the article regarding the correlation of *p16* hypermethylation with astrocytomas versus oligodendrogliomas is well done, with the appropriate controls. However, the second part of the article regarding *p16* as a serum biomarker for diagnosing brainstem gliomas (versus other types of brainstem pathology) is relatively weak and needs additional controls (e.g., measuring serum *p16* methylation in more patients with non-glioma brainstem tumors).

Linda M. Liau
Los Angeles, California

A serum marker for detecting a glioma is a major advance. The authors present some initial data regarding the detection of *p16* promoter methylation. They found an interesting correlation with brainstem tumors. Whether this serum marker can also be used to measure the extent of disease and response to treatment remains to be determined. One can envision the development of a serum test that can obviate the need for brainstem biopsy. This would be a welcomed and important advance in the evaluation of these tumors. I hope the authors continue this work and further refine its application.

Joseph M. Piepmeier
New Haven, Connecticut

Sensitive techniques are now available that can detect aberrant DNA in the serum of cancer patients. The specificity and sensitivity of these assays have been insufficient to warrant their routine clinical use for diagnostic purposes or monitoring treatment response. As these assays improve by selecting more clinically relevant molecular markers and improving sensitivity, it is likely that detection of histologically specific cancers will eventually be accomplished with a simple blood test.

Wakabayashi et al. apply this concept to gliomas by using a modified polymerase chain reaction technique to detect hypermethylation of the *p16* gene in the serum of glioma patients. The *p16* gene was chosen because it is frequently aberrant in astrocytomas and could potentially help to distinguish subtypes of glial tumors. Their tissue analysis showed that hypermethylation of *p16* was significantly more frequent in tumors of astrocytic origin, as compared with oligodendroglial tumors. The serum analysis generally correlated with the tissue results and therefore made it useful for diagnosing gliomas in patients with brainstem lesions as well. Although the results are not sufficiently sensitive and specific to justify the use of this technique on a routine clinical basis, the authors have credibly demonstrated serum molecular diagnosis of gliomas as a proof of principle. These preliminary results should now be tested in a larger series of glioma patients and verified with a suitable cohort of normal controls.

Jeffrey N. Bruce
New York, New York

This is a nicely written report describing the use of methylation-specific polymerase chain reaction to identify methylated *p16* promoter sequences in the serum of patients with astrocytic neoplasms. This work builds upon the observation made by Merlo et al. (1), which demonstrated the presence of *p16* promoter methylation in glial neoplasms, and takes advantage of this finding to explore whether tumor DNA can be detected in the serum of patients with malignant glioma. In a modest number of patients with predominantly astrocytic or oligodendroglial tumors, the authors showed that *p16* promoter methylation is associated mostly with an astrocytic phenotype. This association with phenotype is strengthened greatly by the authors' analysis of 1p/19q loss of heterozygosity, which may be a better marker of lineage than a conventional histological classification.

The implications of this work are that serum *p16* promoter methylation may be a good marker for monitoring tumor status, and possibly for some tumors where biopsy may be associated with an elevated risk of morbidity, a potential substitute to tissue diagnosis. However, a definitive role for use of serum markers to diagnose gliomas will require completion of an appropriately powered prospective trial. That said, the availability of serum markers for monitoring glioma response or progression in relation to anti-tumor therapy would be of tremendous value for the conduct of therapeutic clinical trials and patient decision-making. I look forward to further progress by this group.

Michael A. Vogelbaum
Cleveland, Ohio

1. Merlo A, Herman JG, Mao L, Lee DJ, Gabrielson E, Burger PC, Baylin SB, Sidransky D: 5′ CpG island methylation is associated with transcriptional silencing of the tumor suppressor p16/CDKN2/MTS1 in human cancers. **Nat Med** 1:686–692, 1995.

JOURNAL OF NEUROTRAUMA 26:41–53 (January 2009)
© Mary Ann Liebert, Inc.
DOI: 10.1089/neu.2008.0646

Type I Interferon Inhibits Astrocytic Gliosis and Promotes Functional Recovery after Spinal Cord Injury by Deactivation of the MEK/ERK Pathway

Motokazu Ito,[1] Atsushi Natsume,[1] Hiroki Takeuchi,[1] Shinji Shimato,[2] Masasuke Ohno,[2] Toshihiko Wakabayashi,[2] and Jun Yoshida[1,2]

Abstract

Formation of a glial scar is one of the major obstacles to axonal growth after injury to the adult CNS. In this study, we have addressed this issue by focusing on reactive astrocytes in a mouse model of spinal cord injury (SCI). First, we attempted to identify profile changes in the expression of astrocytic gliosis 10 days after injury by using gliosis-specific microdissection, genome-wide microarray, and MetaCore™ pathway analysis. This systematic data processing revealed many intriguing activated pathways. However, considering that proliferation/mitosis is one of the most prominent features of reactive astrocytes, we focused on the functional role of the Ras-MEK-ERK signaling cascades in reactive astrocytes. SCI-induced proliferation of reactive astrocytes in the lesion is in accordance with the increase in the expression and phosphorylation of MEK-ERK. Second, to reduce reactive gliosis after SCI, liposomes containing the interferon-β (IFN-β) gene were administered locally 30 min after injury. At 14 days after this treatment, GFAP-positive intensity and MEK-ERK phosphorylation at the lesion were reduced. In the animals receiving the IFN-β gene, significant recovery of neurobehavior and parameters of electrophysiology following SCI was revealed by assessments of rotarod performance and improvements in the Basso Mouse Scale for locomotion and cortical motor-evoked potentials. SCI resulted in the degeneration of biotinylated dextran amine-labeled descending corticospinal tract axons, but the IFN-β gene delivery induced regrowth of a large number of corticospinal tract axons. These results suggest that liposome-mediated IFN-β gene delivery inhibits glial scar formation after SCI and promotes functional recovery.

Key words: functional recovery; interferon; microarray; Ras-MEK-ERK pathway; reactive gliosis; spinal cord injury

Introduction

NEUROGENESIS FOLLOWING INJURY in the human adult central nervous system (CNS), along with the subsequent permanent impairment of function is very limited. There have been important advances in understanding the environment that inhibits the regeneration of neurons in mature CNS tissue following injury. One of the major impediments to CNS regeneration is glial scarring, the main component of which is astrocytic gliosis (Stichel and Muller, 1998). Normally, quiescent astrocytes in adults respond vigorously to injury. Some of these responses can have beneficial effects, particularly in the acute phase of injury; they can isolate the injury site and minimize the area of inflammation and cellular degeneration. Some populations of astrocytes might even support axonal regrowth (Faulkner et al., 2004). Eventually, however, they become hypertrophied and proliferative, and they upregulate the expression of glial fibrillary acidic protein (GFAP) and form a dense network of glial processes both at and extending from the lesion site. Spinal cord injury (SCI) is characteristically accompanied by a period of secondary cellular response that occurs in injured tissue after the initial insult. Although the cell biology of the response to SCI is not fully understood, reactive astrocytes are considered to be a prominent feature of the secondary cellular response to SCI. In this study, we attempted to identify the intracellular signaling pathways in reactive astrocytes after SCI in mice by using laser-captured microdissection, followed by a microarray technique comprising 30,000 genes. We then used the web-based functional mapping tool MetaCore™ to

[1]Department of Neurosurgery and [2]Center for Genetic and Regenerative Medicine, Nagoya University School of Medicine, Nagoya, Japan.

identify the genes that are upregulated in the reactive astrocytes of an injured spinal cord; extracellular signal-regulated kinase (ERK) and mitogen-activated ERK-regulating kinase (MEK) were involved in one of the significant pathways for glial scar formation following SCI. The MEK/ERK signaling pathway is fundamental to controlling the development, activation, and proliferation of cells (Pages et al., 1993; Pumiglia and Decker, 1997; Seger and Krebs, 1995; Traverse et al., 1992). This pathway is well conserved among lower and higher eukaryotes, and a modification or dysfunction in this regulatory cascade leads to cellular transformation or uncontrolled proliferation (Brunet et al., 1994; Cowley et al., 1994; Mansour et al., 1994; Okazaki and Sagata, 1995; Seger et al., 1994; Webb et al., 1998).

Type I interferons (IFNs), including IFN-α and IFN-β, are cytokines that exhibit immunomodulatory, cell differentiative, antiangiogenic, and antiproliferative effects, although they have been identified and named based on their actions that "interfere" with viral infections (Borden et al., 2000; Stark et al., 1998). Studies have demonstrated that type I IFNs have multiple functions against various neoplasms, particularly glial tumors. In the past two decades, due to these pleiotropic biological effects, there have been major achievements in understanding the signaling mechanism through which type I IFNs exert their effects. Since the original discovery of the classical Janus-activated kinase (JAK)/signal transducer and activator of transcription (STAT) pathways, it has become clear that the coordination and cooperation of multiple distinct signaling cascades, including the MEK/ERK cascade, are required for generating the response to IFNs.

In this study, we demonstrate that the expression of vector-mediated murine IFN-β inhibits glial scar formation after SCI and promotes functional recovery by targeting the MEK/ERK pathway. These results shed some light on the mechanism of glial scarring following CNS injury and may indicate a potential therapeutic approach for this debilitating injury.

Methods

Construction of murine IFN-β-expressing cationic liposomes

Liposomes are artificial lipid bilayer vesicles considered to be useful drug delivery systems. We found that cationic liposomes comprising N-(α-trimethylammonioacetyl)-didodecyl-D-glutamate chloride, dilauroylphosphatidylcholine, and dioleoyl phosphatidylethanolamine provide high-efficiency DNA entrapment and a high potential for DNA transfer to dividing cells, particularly cancer cells (Yoshida and Mizuno, 2003). In this study, we prepared two types of liposomes: one containing the plasmid vector pSV2muIFN-β that expresses murine (mu) IFN-β under the SV40 early promoter, and the other containing the plasmid vector pCH110 that was constructed by the fusion of the *E. coli lacZ* (β-galactosidase) gene to the SV40 early promoter (GE Healthcare, Little Chalfont, U.K.), as described previously (Natsume et al., 1999). These liposome vectors were designated as lip(pSV2muIFN-β) and lip(pCH110), respectively.

Surgical procedures

Adult female C57BL/6 mice (8–12 weeks old; SLC, Shizuoka, Japan) were used in this study. All experiments were carried out in accordance with the ethical guidelines of the Nagoya University Institutional Animal Care and Use Committee. The mice were anesthetized with 1.5% halothane and maintained on 1.25% halothane in a oxygen/nitrous oxide gas mixture. Laminectomy was performed at vertebral level T9–T10. The dura was opened, and the dorsal half of the spinal cord was transected to a depth of 1 mm with a pair of extra-fine microscissors. The animals were divided into four groups: group A, laminectomy only; group B, plain spinal cord injury; group C, spinal cord injury with lip(pCH110) delivery; and group D, spinal cord injury with lip(pSV2muIFN-β) delivery. At 30 min post-injury, either lip(pCH110) or lip(pSV2muIFN-β) (40 nmol of lipid and 0.8 μg of DNA in 10 μL of phosphate-buffered saline [PBS]) was injected locally into the lesion cavity with a glass micropipette. This injection procedure did not induce secondary damage to the spinal cord. The overlying muscle and skin were sutured. The mice were placed on soft bedding on a warming blanket held at 37°C for 1 h after surgery.

Laser-captured microdissection and microarray

On day 10 after surgery, five animals from the laminectomy only and plain SCI groups, were deeply anesthetized with barbiturate overdose and intracardially perfused with PBS. Their spinal cords were removed and immediately frozen in Tissue-Tek OCT embedding medium (Sakura Finetek, Tokyo, Japan). The spinal cords were sectioned in the sagittal plane onto uncoated slides. A PixCell II LCM instrument (Arcturus, Mountain View, CA) was used to dissect the injury site, and RNA was extracted from the microdissected samples by using the PicoPure RNA Isolation Kit (Arcturus), according to the manufacturer's instructions. Total RNA was pooled from five animals from each group; it was then amplified and labeled using the Amino Allyl MessageAmp aRNA Kit (Ambion, Austin, TX). Briefly, after performing reverse transcription reactions (2 μg of total RNA/sample), double-stranded cDNA was transcribed *in vitro* by using the amino allyl cRNA. The RNA was amplified twice. The purified and concentrated cRNA (5 μg) was coupled with either Cy3 or Cy5 dyes (GE Healthcare). The dye-labeled aRNA was purified from uncoupled dye by using Micro Bio-Spin P-30 Tris chromatography columns (Bio-Rad, Hercules, CA) and Microcon YM-30 centrifugal filter devices (Millipore, Billerica, MA). The cRNA was fragmented in a fragmentation buffer (40 mmol/L Tris-acetate [pH 8.1], 100 mmol/L potassium acetate, and 30 mmol/L magnesium acetate) at 94°C for 15 min and purified with Microcon YM-10 (Millipore). An oligonucleotide-based mouse DNA microarray, AceGene (mouse Oligo Chip 30K; http://hitachisoft.jp/dnasis/ex_acegene/index.html; DNA Chip Research, Yokohama, Japan) was preblocked with 1% bovine serum albumin (BSA) solution. The fragmented cRNA was added to the microarray in hybridization solution and subsequently hybridized at 42°C for 16 h. The arrays were then washed, scanned at a pixel size of 10 μm, gridded, and analyzed (GenePix 4000B; Axon Instruments, Union City, CA). The background was subtracted, and the medium sum intensity (CH1 and CH2) of <100 absorbance units was excluded. Data were normalized by the trimmed mean at 10% to account for the differences in the amounts of labeled RNA or labeling efficiencies.

Pathway analysis

We next attempted to identify novel gene networks involving biological pathways in reactive astrocytes after SCI. For this purpose, we analyzed the genes whose expressions were upregulated in the lesion by at least a factor of 2.0, relative to the respective expressions in the normal cord, by using a functional mapping tool, MetaCore™ (GeneGO, St Joseph, MI). MetaCore is a web-based computational platform designed primarily for the analysis of high-throughput experimental data in the context of mouse regulatory networks and pathways. It includes a curated database of protein interactions, metabolism, and bioactive compounds. For a network of a particular size, MetaCore can be used to calculate the statistical significance based on the probability of the network's assembly from a random set of nodes (genes) that is of the same size as the input list (p value).

Semiquantitative reverse transcriptase polymerase chain reaction (RT-PCR)

Eight genes from the microarray experiment were selected for validation by semiquantitative RT-PCR. Based on the results of pathway analysis, we selected genes that were included in the three pathways with the lowest p value. The names and primer sequences of the selected genes are listed in Table 1. The total RNA extracted from the laser-captured tissues was subjected to DNase (Invitrogen, Carlsbad, CA) treatment prior to reverse transcription by using a Transcriptor First-Strand cDNA Synthesis Kit (Roche, Mannheim, Germany), according to the manufacturer's protocol. PCR amplification was performed using GoTaq DNA polymerase (Promega, Madison, WI). The cycling parameters were as follows: denaturation at 95°C for 45 sec, primer annealing at 55°C for 45 sec, and 25 cycles of extension at 72°C for 60 sec. PCR cycling was preceded by an initial denaturation at 95°C for 2 min, followed by final extension at 72°C for 5 min. The PCR products were loaded on a 1.5% agarose gel and stained with ethidium bromide. Band intensities were quantified by densitometric scanning by using the NIH IMAGE program. The results were evaluated semiquantitatively by comparison with the relative amounts of β-actin PCR products.

Primary astrocyte culture and treatment with liposome/plasmid-expressing murine IFN-β

We examined whether liposome-mediated IFN-β gene delivery exhibits a growth inhibitory effect on proliferating astrocytes. Primary cell cultures of astrocytes were prepared from the cerebral hemispheres of fetal C57BL/6 mice (SLC). The hemispheres were cleaned off the meninges and the choroid plexus and digested with 0.1% trypsin (Invitrogen) in PBS for 30 min at 37°C. The tissue was washed with Dulbecco's minimal essential medium (DMEM; Invitrogen) with 1% glucose and 10% fetal calf serum (FCS), followed by 5 min of incubation with 1% DNase I in PBS at room temperature. The samples were dissociated in DMEM containing 10% FCS, 1% nonessential amino acids (Invitrogen), penicillin (50 μg/mL), streptomycin (50 μg/mL), and glutamine (2 nM). The suspension containing 1×10^5 cells was seeded onto 35-mm poly-L-lysine-coated Petri dishes. All cells were immunocytochemically confirmed as glial cells based on their expression of GFAP. On the next day, the cells were treated with lip (pSV2muIFN-β) (20 nmol lipid and 0.4 μg DNA/mL), lip (pCH110) (20 nmol lipid and 0.4 μg DNA/mL), liposome alone (20 nmol lipid/mL), pSV2muIFN-β alone (0.4 μg DNA/mL), muIFN-β (100 IU/mL), or PBS. After 2 days, the cells were immunostained with anti-GFAP Ab and then with Alexa 488-labeled IgG. The total number of GFAP-positive cells was counted.

Western blotting

In order to evaluate differential expression of GFAP and MEK/ERK between the normal cord and the lesion transfected with either *lacZ* or IFN-β vectors (five animals each), the scar captured by laser-captured microdissection was lysed with a cell lysis buffer (Cell Signaling Technology, Inc., Beverly, MA) containing 1 mM phenylmethylsulfonylfluoride, 10 μg/mL aprotinin, leupeptin, pepstatin, and 50 mM sodium

TABLE 1. PRIMER SEQUENCES

Genes		*Sequence*
β-actin	Forward	5′-GACATGGAGAAGATCTGGCACCACA-3′
	Reverse	5′-ATCTCCTGGTCGAAGTGTAGAGCAA-3′
Fibronectin	Forward	5′-GGCTGGCGCTGTGACAA-3′
	Reverse	5′-TCGAGAATCGTCTCTGTCAGCTT-3′
MMP9	Forward	5-′AAGTGGGACCATCATAACATCACA-3′
	Reverse	5′-CGCTTCGGGTCCGTACAC-3′
TIMP	Forward	5′-CCACCTTATACCAGCGTTAT-3′
	Reverse	5′-CTGGGACTTGTGGGCATATC-3′
GFAP	Forward	5′-GATGTCTACCAGGCGGAGCTT-3′
	Reverse	5′-CTGTCTATACGCAGCCAGGTTGT-3′
MEK1	Forward	5′-TGGCAATTTTTGAGTTGTTGGA-3′
	Reverse	5′-CCTCGGCGTCAGATCTTTTG-3′
MEK2	Forward	5′-CCAGTGGTGTGTTCAGCTCAGA-3′
	Reverse	5′-GTGTGCTGGGCTGCTTCAG-3′
ERK1	Forward	5′- GCACCAACCATTGAGCAAATG-3′
	Reverse	5′-CTTGAGGTCACGGTGCAGAA-3′
ERK2	Forward	5′CTCCTGCTGAACACCACTTGTG-3′
	Reverse	5′-ACCCTTGGAATTCAACATAATTTCTG-3′

fluoride. Protein samples (30 μg) were denatured at 100°C for 5 min and subsequently applied to each well and electrophoresed on a 12.5% polyacrylamide gel. After the proteins were transferred to a polyvinylidene difluoride membrane, it was blocked with 3% low-fat skim milk, incubated with primary Abs against GFAP (1:500; DakoCytomation, Glostrup, Denmark), ERK-1 (C-16, 1:500; Santa Cruz Biotechnology, Santa Cruz, CA), MEK-1 (C-18, 1:500; Santa Cruz Biotechnology), phospho-ERK1/2 (p44/42 MAP Kinase, Thr202/Tyr204, 1:500; Cell Signaling, Danvers, MA), and phospho-MEK1/2 (Ser217/221, 1:500; Cell Signaling), and then washed and incubated with a horseradish peroxidase–labeled secondary Ab. Visualization was performed using an enhanced chemiluminescence technique.

Transgene expression at injury site

For the detection of *lacZ* gene expression, we injected lip(pCH110) (40 nmol of lipid and 0.8 μg of DNA in 10 μL of PBS) locally at the injury site using the aforementioned method. After 4 days, the mice were killed and their spinal cords were removed and frozen in Tissue-Tek OCT embedding medium. The frozen sections (20 μm) were fixed in 2.5% glutaraldehyde in PBS and stained with X-gal before counterstaining with hematoxylin. For the detection of muIFN-β expression, Western blotting was performed using the laser-captured tissue 4 days after either lip(pSV2-muIFN-β) or lip(pCH110) injection, as described above. We used sheep anti-mouse IFN-α/β polyclonal antibody (1:1000 dilution; PBL Biomedical Laboratories, New Brunswick, NJ) preabsorbed overnight at 4°C by 100 μg of normal spinal cord lysate in 1% BSA/5% skim milk in PBS as a primary antibody. The membrane was stained with Coomassie blue to confirm that an equal amount of protein had been loaded in each lane.

Immunohistochemistry and immunofluorescence

Three mice were deeply anesthetized with barbiturate overdose and intracardially perfused with PBS followed by 4% paraformaldehyde (PFA) in 0.1 M phosphate buffer. The spinal cord that contained the lesion was removed and postfixed overnight in the same fixative. The fixed tissues were embedded in paraffin, and 10-μm sections were prepared for immunohistochemistry. The paraffin sections were deparaffinized in two changes of xylene and then rehydrated. After washing in PBS, the sections were blocked with 0.5% BSA in PBS. Rabbit anti-GFAP (1:200; DakoCytomation) was used as the primary antibody. The sections were incubated with the primary antibody for 1 h at room temperature and then immersed in 0.3% hydrogen peroxide in absolute methanol for 15 min to block endogenous peroxidase. After washing three times in PBS, the sections were incubated with the corresponding biotinylated secondary Abs for 30 min at room temperature. Diaminobenzidine (DAB) solution was used as the chromogen, and the sections were counterstained with hematoxylin.

For immunofluorescence, fresh frozen sections (15 μm) of the spinal cord were fixed in 4% PFA. After rinsing three times in PBS, the sections were blocked and permeabilized in 0.5% BSA and 0.5% Triton X-100 in PBS for 60 min. The samples were then incubated overnight at 4°C with primary Abs against phospho-ERK1/2 (p44/42 MAP kinase, Thr202/Tyr204, 1:100; Cell Signaling) and GFAP (1:200; DakoCytomation). Phospho-ERK1/2 was detected with Alexa 488-labelled IgG (1:200; Molecular Probes, Eugene, OR), and GFAP was detected with Alexa 546-labeled IgG (1:200). The sections were analyzed using an Olympus FV5-PSU confocal laser microscope (Olympus, Tokyo, Japan).

Anterograde tracing

On day 14 after the dorsal hemisection, three mice were anesthetized with an IP injection of pentobarbital (60–70 mg/kg body weight). To trace the descending corticospinal tract (CST) axons, biotinylated dextran amine (BDA) (Molecular Probes) was injected into the somatomotor cortex with a 10-μL Hamilton microsyringe fitted with a pulled glass micropipette. Three injections were administered 1.0 mm lateral to the midline at 0.5 mm anterior, 0.5 mm posterior, and 1.0 mm posterior to the bregma, to a depth of 0.5 mm from the cortical surface (Inman and Steward, 2003). The mice were sacrificed humanely by anesthetic overdose at 14 days post-injection. They were perfused transcardially with 4% PFA; the vertebral columns were removed and postfixed by immersion for 24 h in the same fixative. The spinal cords were cryoprotected in 20% sucrose and then frozen in Tissue-Tek OCT embedding medium. The cords were sectioned along the sagittal plane onto poly-L-lysine-coated slides. After washing three times in PBS and 0.1% Triton X-100, the sections were incubated for 1 h with avidin and biotinylated horseradish peroxidase (Molecular Probes), washed again three times in PBS, and reacted with DAB in 50 mM Tris-buffer (pH 7.6) and 0.024% hydrogen peroxide. The sections were examined under a BIOZERO fluorescent microscope (Keyence, Osaka, Japan). BDA-positive fibers were traced on translucent graph sheets at approximately 100× magnification using a camera lucida. The total number of traced axons 1.0 mm rostral and 0.5 mm caudal to the lesion site was counted, and the length of the longest axon was measured. Five sections sampled from each animal were evaluated. The number of axons on the caudal side was expressed as the percentage of the number of axons on the rostral side.

Basso Mouse Scale for locomotion

We measured the recovery of hindlimb motor functions in eight mice in each treatment group by using the Basso Mouse Scale (BMS) for locomotion, as previously described (Basso et al., 2006). The behavior of each animal was videotaped for 5 min, and two investigators provided a score (on a scale of 0–9) for each hindlimb at 4, 7, 14, 21, and 28 days after SCI. The scores from the two hindlimbs were averaged to obtain a single value per animal for each time point.

Rotarod testing

First, the mice were individually trained to walk rotarod daily for 5 days before the hemisection. To assess balance and ability to coordinate stepping, eight animals in each group were placed on a single-lane rotarod treadmill (MK600; Muromachi Kikai, Tokyo, Japan) for three trials per session. The rotarod was set to constant acceleration, and the animals were scored based on the number of rotations it took for them to fall.

Electrophysiology

To measure signal conduction in the motor pathways after SCI, transcranial electrical motor nerve evoked-action potentials (MEPs) were measured from 28 days after injury. To record MEPs, the mice were anesthetized with 1.5% halothane and maintained in 1.0% halothane in an oxygen/nitrous oxide (30%/70%) gas mixture. All recordings were performed using a standard clinical electromyographical analytical method with a 3000-Hz hi-cut filter and a 30-Hz low-cut filter (Nihon Kohden, Tokyo, Japan) and needle electrodes. Electrical stimulation (1 Hz, 6 mA) was delivered over the cranium at an area 1 mm lateral to the bregma. Evoked responses were recorded from the contralateral femoral muscle. Latency was defined as the time elapsed between stimulus onset and the initial deflection of the response from baseline (point 3 in Fig. 7). The amplitude was measured from base to peak (from points 3 to 4 in Fig. 7).

Statistical analysis

The statistical significance of the differences observed was determined by ANOVA (StatView; SAS Institute, Cary, NC), and Bonferroni's correction was employed for multiple comparisons.

Results

Molecular signaling of reactive astrocytes following SCI

A laser-captured microdissection technique was used to procure specific areas from the heterogenously damaged tissue structure. In order to analyze the molecular signaling of reactive astrocytes following SCI, the lesioned site expected to form a glial scar was captured, and the expressions of 30,000 genes were profiled by a microarray on day 10 after dorsal hemisection of the spinal cord at the T9–T10 level. We evaluated gene expressions as either significantly upregulated or significantly downregulated by using the fold-level criteria (>2-fold change: the significance of upregulation was set at >2 and that of downregulation at <0.5.). Data analysis identified 488 significantly upregulated genes and 226 downregulated genes in several different categories. Complete lists of genes demonstrating significant expression changes are listed in Supplementary Table 1 (online only). Only 1.6% of the probe set corresponding to individual genes was expressed at a level >2.0-fold after SCI. After the microarray data were imported into MetaCore, functional gene networks were generated to integrate reactions and interactions around the identified genes of interest. Significantly activated

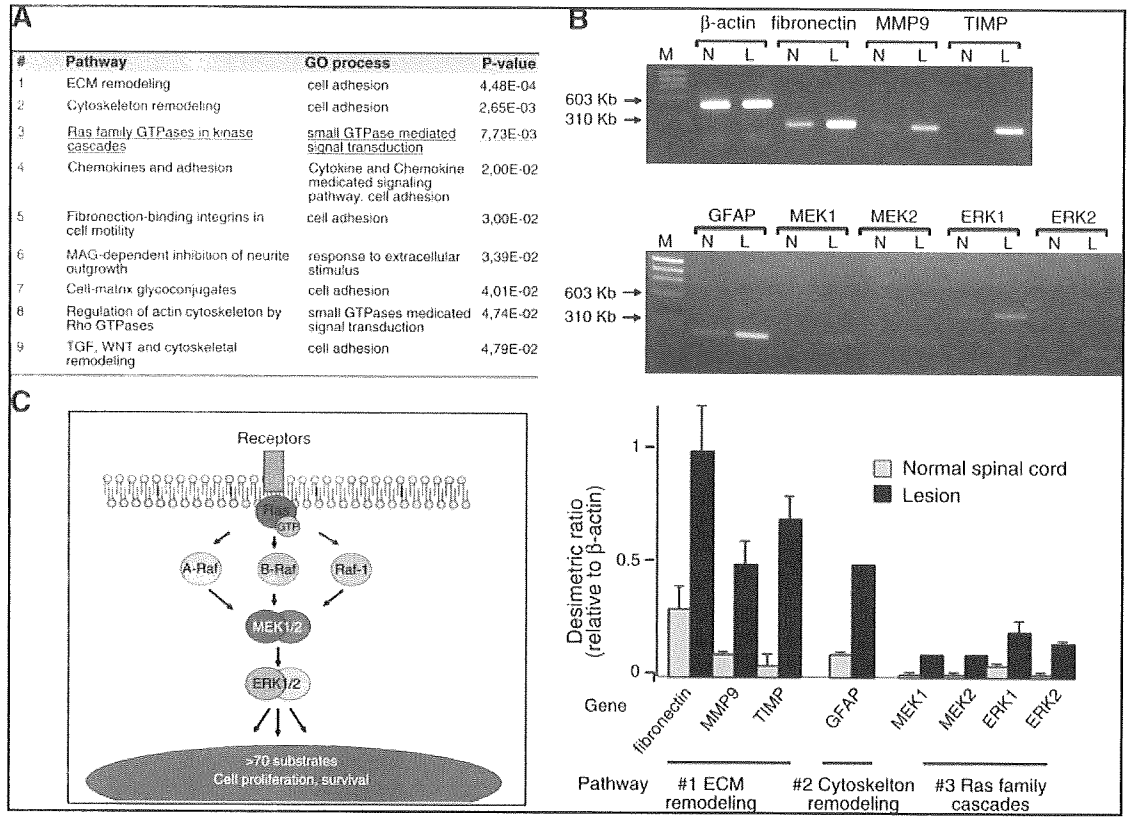

FIG. 1. Molecular signaling of reactive astrocytes following SCI. (**A**) Significantly activated pathways identified by MetaCore are listed. (**B**) We selected specific genes from the pathways of interest and verified their expression changes by using semiquantitative RT-PCR. The histogram shows the amount of mRNA expression, relative to that of β-actin expression. Columns represent the mean values from three independent experiments. Bars indicate SD. M, marker; N, normal spinal cord; L, lesion. (**C**) Ras family cascades.

pathways are displayed in Fig. 1A ($p < 0.05$). This secondary data processing yielded many intriguing profiles of gene activity in reactive astrocytes following SCI, such as extracellular matrix (ECM) and cytoskeleton remodeling and myelin-associated glycoprotein (MAG)-dependent inhibition of neurite outgrowth. We selected specific genes from pathways of interest and verified their expression changes by using semiquantitative RT-PCR (Fig. 1B). In this paper, we have focused on the most interesting pathway—Ras family cascades (Fig. 1C); the other pathways will be reported comprehensively in different articles. The semiquantitative RT-PCR revealed that MEK1/2 and ERK1/2 expressions were markedly upregulated in the lesion (Fig. 1B).

Liposome-mediated IFN-β gene delivery inhibits growth of primary cultured astrocytes

As shown in Fig. 2, the liposome/IFN-β gene complex, lip(pSV2muIFN-β), suppressed the growth of astrocytes significantly when compared with the relevant matched control [lip(pCH110)]. The other control agents did not exhibit a suppressive effect (data not shown). The effect of lip(pSV2-muIFN-β) was considered to be cytostatic but not cytocidal, based on the facts that the number of GFAP-positive cells with lip(pSV2muIFN-β) treated on day 3 was similar to that seen on day 1, and that no dead cells were observed in the lip(pSV2muIFN-β)-containing culture.

Liposomes can effectively deliver transgenes to injured spinal cord in mice

In order to evaluate the transduction efficiency of liposomes containing a foreign gene into the injured spinal cord *in vivo*, a *lacZ*-expressing liposomal vector was injected locally into the lesioned site 30 min after SCI. The expression of β-galactosidase *in vivo* was examined histologically 4 days after lip(pCH110) (40 nmol of lipid and 0.8 μg of DNA in 10 μL of PBS) was injected into the injury site, and its expression was demonstrated at the injured site by X-gal staining (Fig. 3A). In addition, the laser-captured SCI site exhibited the expression of muIFN-β 4 days after lip(pSV2muIFN-β), but not after the control vector (Fig. 3B).

Liposome-mediated IFN-β gene delivery decreases intensity of reactive glial scar formation following SCI, and deactivates the MEK-ERK pathway

The liposomal IFN-β vector or the control *lacZ* vector was injected into the lesioned spinal cord 30 min after dorsal hemisection. On day 14, the expression of GFAP and ERK/MEK at the lesion site was evaluated by Western blotting and histology (Fig. 4). We observed an increase in the level of GFAP and the total amount of ERK1/MEK1 in the lesion receiving the *lacZ* vector, which is consistent with our RT-PCR study shown in Fig. 1B. Moreover, the level of active ERK/MEK (i.e., phospho-ERK1/2 and phospho-MEK1/2) also increased in the lesion, compared to that in a normal spinal cord. On the other hand, IFN-β gene delivery decreased the expression level of GFAP and the total amounts of ERK/MEK and phosphorylated ERK/MEK. Immunohistochemistry exhibited a decrease in the number of GFAP-positive cells in the lesion receiving the IFN-β gene (Fig. 4B). The individual cells in the IFN-β-treated spinal cord were weakly stained with GFAP, when compared to the cells in the control (*lacZ*-treated group). These findings suggested that

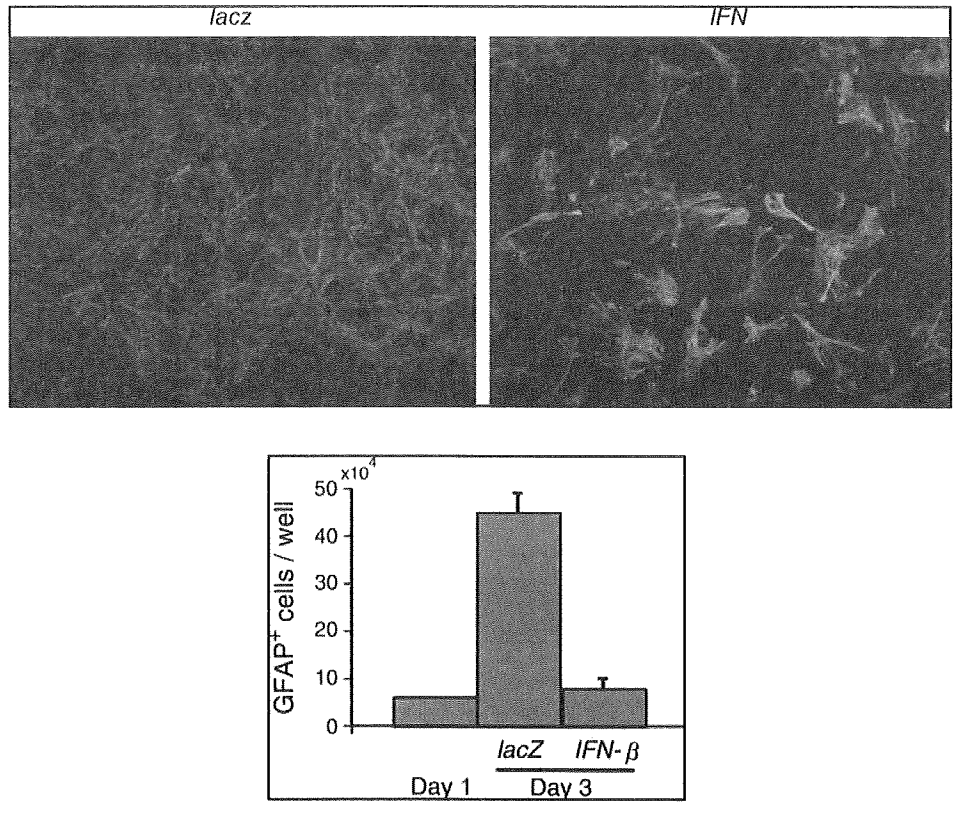

FIG. 2. Liposome-mediated IFN-β gene delivery inhibits the growth of primary cultured astrocytes. The liposome/IFN-β gene complex delivery suppressed the growth of astrocytes significantly, compared to the control *lacZ* delivery.

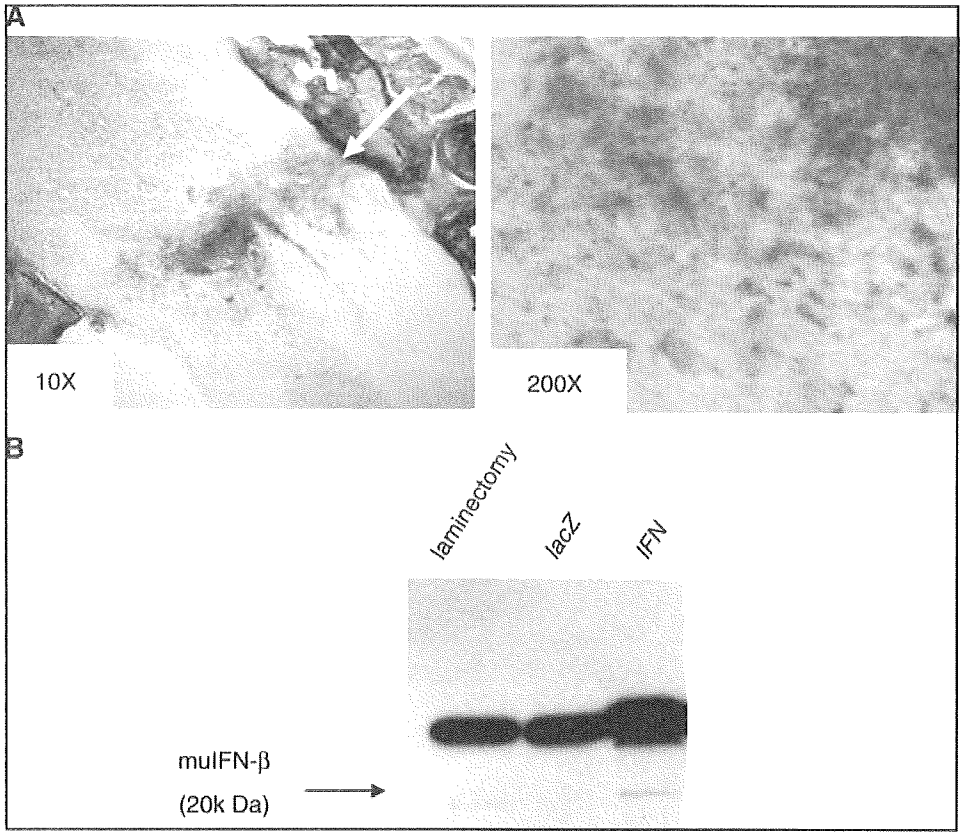

FIG. 3. Liposomes can effectively deliver transgenes to the injured spinal cord in mice. (**A**) The expression of β-galactosidase *in vivo* was examined histologically 4 days after *lacZ*-expressing liposomal vector (40 nmol of lipid and 0.8 μg of DNA in 2 μL of PBS) was injected into the injury site. β-Galactosidase expression was demonstrated at the injured site by X-gal staining. The arrow indicates the injured site. (**B**) By Western blotting, the expression of murine IFN-β was demonstrated in the laser-captured lesion 4 days after injection of the IFN-β-expressing vector, but not in the normal spinal cord receiving only laminectomy, and in the lesion injected with the *lacZ*-expressing vector.

glial scar formation was suppressed after IFN-β gene delivery. Moreover, double-labeling confocal experiments revealed colocalization of GFAP and phospho-ERK1/2 in the lesion, and the deactivated MEK/ERK in the lesion receiving the IFN-β gene, compared to the lesion receiving the *lacZ* gene (Fig. 4C). To exclude the possibility of autofluorescence of the lesioned tissue, the relevant sections were stained with the secondary antibodies (insets in Fig. 4C).

Regenerative sprouting of CST axons following IFN-β gene delivery

After 14 days of dorsal hemisection, BDA was injected into the somatomotor cortex to trace the descending CST axons. Fourteen days later, BDA-labeled axons were visualized by DAB (Fig. 5). In the *lacZ*-treated animals, most BDA-labeled axons ended at about 100 μm rostral to the edge of the injury. Almost no CST axons were observed at both the lesioned and caudal areas (approximately 1% compared to those seen at the rostral side). In contrast, the IFN-β vector, lip(pSV2muIFN-β), increased the number of BDA-labeled axons at the site 0.5 mm caudal to the lesioned area (approximately 15% of that at the rostral side). The distance between the caudal-most terminus of individual CST axons and the lesion margin was measured, and the average distance was found to be 0.87 mm. Hence, liposome-mediated IFN-β gene delivery promoted axonal elongation of the injured CST axons.

Behavioral studies

To determine whether IFN-β gene delivery improved recovery of function after SCI, we assessed functional recovery using two independent behavioral tests, namely the BMS score and the rotarod test. All neurobehavioral assessments were undertaken by observers who were blinded to the experimental groups. BMS was performed for open-field hindlimb locomotor function assessment (Fig. 6A). All injured animals except those in the laminectomy group exhibited a mean BMS score of 2; this indicated extensive ankle movement on the first day after SCI. Animals with plain SCI receiving no agents (plain SCI group) and those receiving the *lacZ* control vector (*lacZ*-treated group) spontaneously recovered to a BMS score of 3–4 (plantar placing of the paw or occasional plantar stepping) until 14 days post-injury; no further recovery was observed thereafter. On the other hand, the IFN-β-treated animals showed a significant improvement in BMS scores relative to the control groups. Differences between the mean BMS of the IFN-β-treated group and the other groups were statistically significant 21 days post-injury and thereafter ($p < 0.05$). On average, the IFN-β-treated group exhibited a mean BMS of 7.1 ± 1.1 at 28 days, while the plain SCI and the *lacZ*-treated groups attained a mean score of 4.2 ± 0.3 and 3.1 ± 0.7, respectively.

Rotarod analysis was performed to examine another locomotor function post-SCI (Fig. 6B). During the preoperative training period, all the mice could walk the rotarod without falling. The animals were evaluated for locomotor recovery on days 1, 4, 7, 14, 21, and 28. There was significant recovery of performance over 14 days post-injury in the IFN-β-treated group, while the performance was severely impaired in the plain SCI and *lacZ*-treated animals at all time points ($p < 0.05$). None of the groups recovered to preinjury levels of performance.

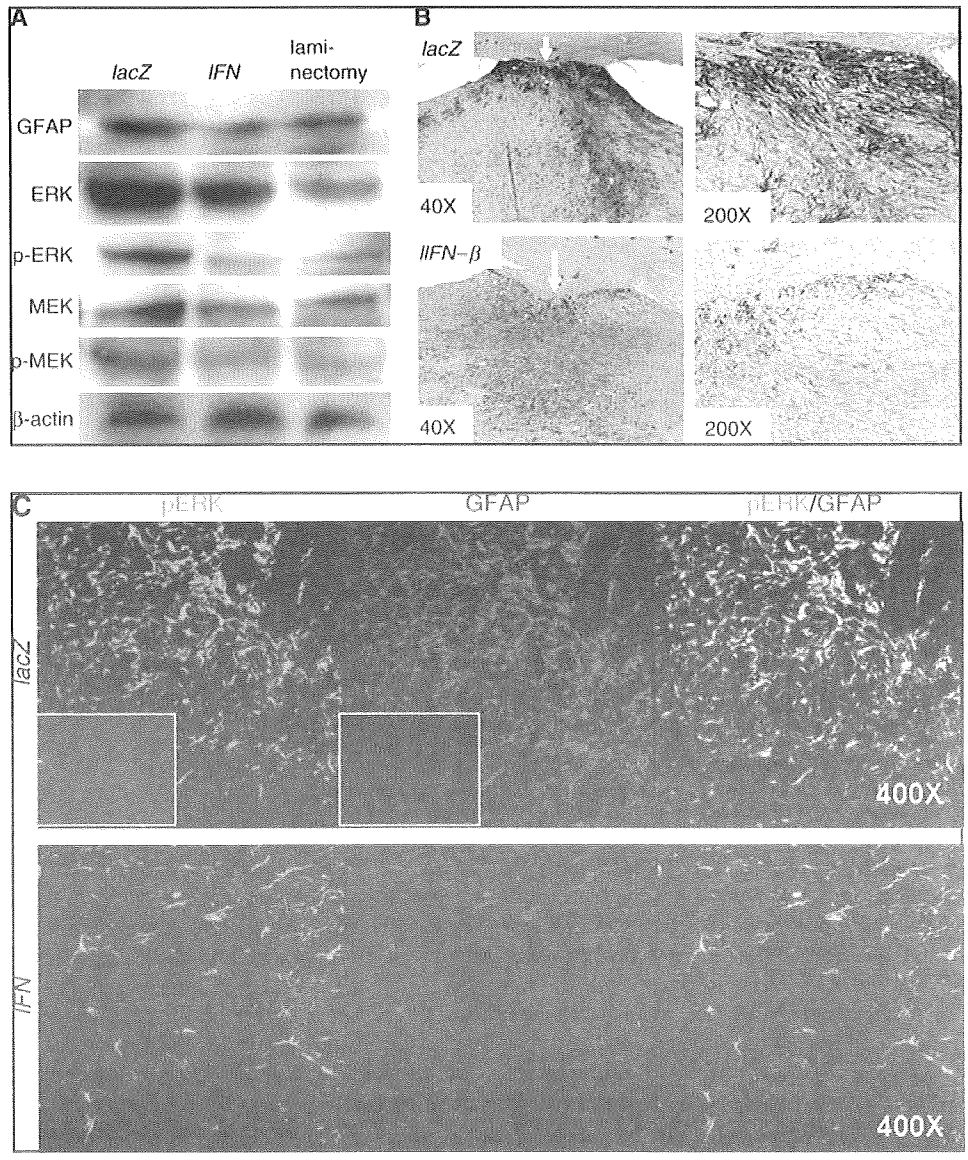

FIG. 4. Liposome-mediated IFN-β gene delivery decreases the intensity of reactive glial scar formation following SCI and deactivates the MEK-ERK pathway. (A) The level of GFAP and total amount of ERK1/2 and MEK1/2 were increased in the lesion receiving the *lacZ* vector, compared to normal tissue that received laminectomy only. Moreover, the levels of phospho-ERK1/2 (p-ERK) and phospho-MEK1/2 (p-MEK) also increased in the lesion. On the other hand, the IFN-β gene delivery significantly decreased the expression level of GFAP and the total amount of ERK/MEK as well as phospho-ERK/MEK. (B) The liposomal IFN-β vector or the control *lacZ* vector was injected into the lesioned spinal cord 30 min after dorsal hemisection. On day 14, GFAP-positive astrocytes at the lesion site were evaluated. The IFN-β gene delivery decreased the intensity of reactive glial scar formation following SCI. The arrow indicates the injured site. (C) In the SCI animals, the GFAP-positive cells were densely double stained with antibodies to phospho-ERK1/2 (pERK). The liposomal IFN-β vector decreased the number of double-stained cells in the lesion. To exclude the possibility of nonspecific staining of the destroyed tissue, the relevant sections were stained with secondary antibodies (insets). (Color image is available online at www.liebertpub.com/jon)

Electrophysiology

Measurement of the motor nerve evoked-action potential revealed prolonged latency and a marked decrease in the action potential amplitude in animals with plain SCI or those treated with the *lacZ* control vector (Fig. 7). The latency was prolonged from 1.63 msec in the laminectomy group to 2.39 msec and 2.78 msec in the plain SCI and *lacZ*-treated groups, respectively. Further, the amplitude was reduced from 18.95 μV in the laminectomy group to 6.8 μV and 6.7 μV in the plain SCI and *lacZ*-treated groups, respectively. In animals treated with the IFN-β gene, both latency and amplitude recovered to 2.05 msec and 9.87 μV, respectively ($p < 0.05$).

Discussion

In this study, we examined the astrocyte response that accompanies SCI. A GeneChip screening of laser-microdissected scar tissue following SCI provided a list of several hundred genes that are upregulated over a 2- to 55-fold range. Based on the hypothesis that major astrocytic responses to injury include hypertrophy and proliferation, we focused on stimulating the ERK pathway. Using liposome-mediated gene delivery, we suggested that IFN-β delivery had a dramatic effect on the reduced expression of GFAP, glial scarring, and a concomitant increase in axonal outgrowth and functional recovery.

SCI remains essentially untreatable and developing new therapies for its treatment is extremely important. This study addresses an extremely important issue, i.e., regeneration beyond the glial scar. The multifaceted roles of astrocytes, which respond to SCI, have recently been studied. Faulkner and associates demonstrated that selective depletion or ablation of the subpopulation of reactive astrocytes caused widespread tissue disruption and pronounced cellular

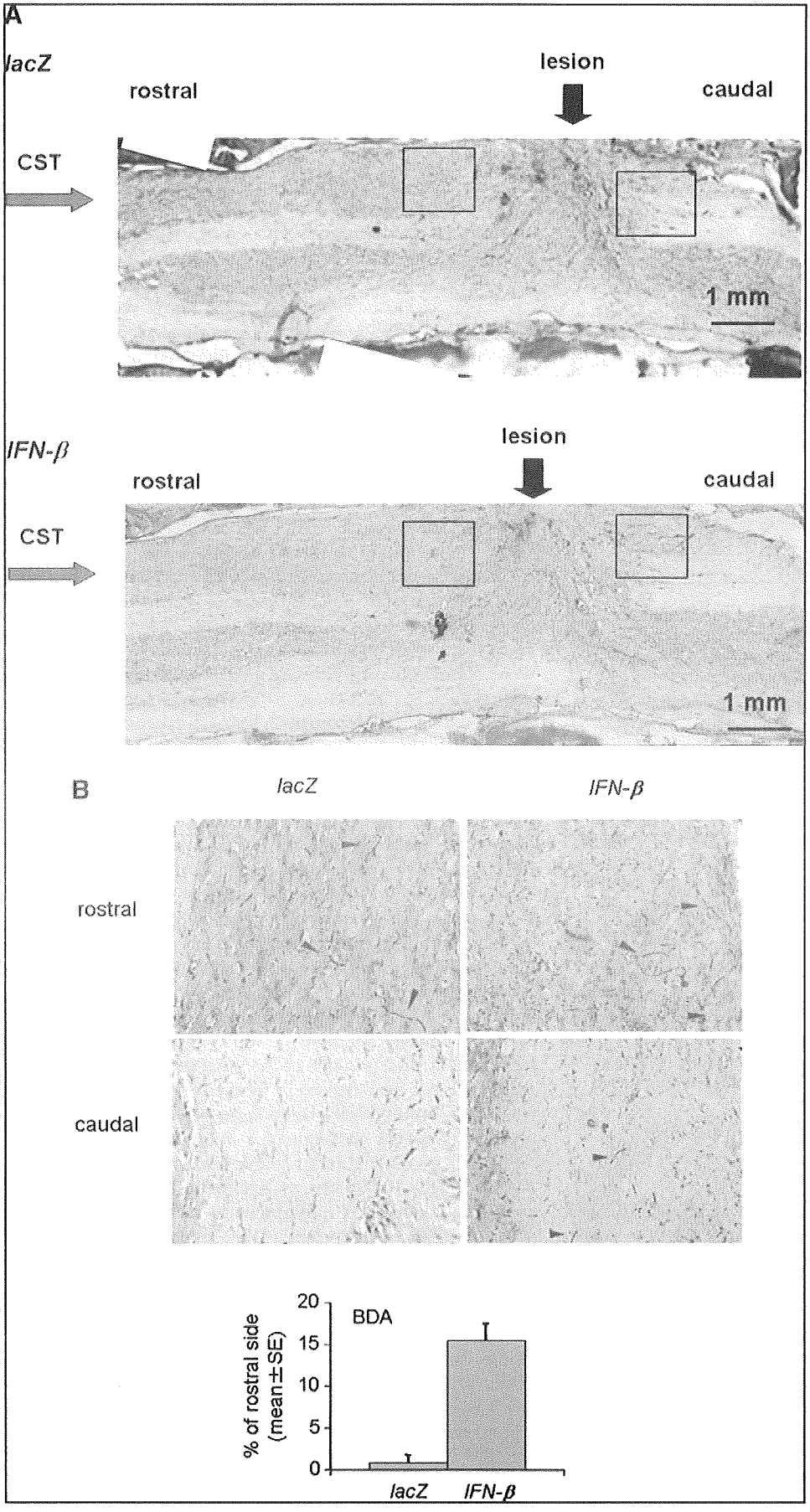

FIG. 5. Regenerative sprouting of the CST tract axons following IFN-β gene delivery. After 14 days of dorsal hemisection, BDA was injected into the somatomotor cortex to trace the descending CST axons. At 14 days after the injection, BDA-labeled axons were visualized by DAB. In the *lacZ*-treated animals, most BDA-labeled axons ended at about 100 μm rostral to the edge of the injury. Almost no CST axons were observed at both the lesioned and caudal areas (approximately 1% of those seen at the rostral side). In contrast, the IFN-β-expressing vector, lip(pSV2muIFN-β), increased the number of BDA-labeled axons at the site 0.5 mm caudal to the lesioned area (approximately 15% of that at the rostral side). (A) Longitudinal planes of the spinal cord receiving the *lacZ* or IFN-β gene vector (arrows indicate the CST and lesioned site). (**B**) High-magnification images of the areas boxed in part A. The arrowheads indicate BDA-labeled axons. (Color image is available online at www.liebertpub.com/jon)